

**THE UNIVERSITY OF TURKISH AERONAUTICAL ASSOCIATION  
INSTITUTE OF SCIENCE AND TECHNOLOGY**

**NUMERICAL ANALYSIS OF THERMAL PERFORMANCE FOR  
PARABOLIC TROUGH SOLAR COLLECTOR USING  $Al_2O_3$  NANO-FLUID**

**Master Thesis**

**RAHELL M.R**

**Mechanical and Aeronautical Engineering Department**

**Master Thesis Program**

**May, 2017**

**THE UNIVERSITY OF TURKISH AERONAUTICAL ASSOCIATION  
INSTITUTE OF SCIENCE AND TECHNOLOGY**

**NUMERICAL ANALYSIS OF THERMAL PERFORMANCE FOR  
PARABOLIC TROUGH SOLAR COLLECTOR USING  $Al_2O_3$  NANO-FLUID**

**MASTER THESIS**

**Rahell M.R**

**1403730006**

**Mechanical and Aeronautical Engineering Department**

**Master Thesis Program**

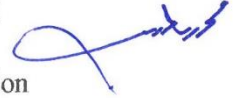
**Supervisor: Assist. Prof. Dr. Mohamed Salem Elmnefi**

Rahell M.R, having student number 1403730006 and enrolled in the Master Program at the Institute of Science and Technology at the University of Turkish Aeronautical Association, after meeting all of the required conditions contained in the related regulations, has successfully accomplished, in front of the jury, the presentation of the thesis prepared with the title of: Numerical Analysis of Thermal Performance for Parabolic Trough Solar Collector Using Al<sub>2</sub>O<sub>3</sub> Nano-Fluid.

**Supervisor:**

Assistant Prof. Dr. **Mohamed Salem ELMNEFI**

The University of Turkish Aeronautical Association



**Jury Members:**

Assistant. Prof. Dr. **Sinan KÖRPE**

The University of Turkish Aeronautical Association



Assistant Prof. Dr. **Munir ELFARRA**

Ankara Yildirim Beyazit University



**Thesis Defense Date:** 15.05.2017

**THE UNIVERSITY OF TURKISH AERONAUTICAL ASSOCIATION  
INSTITUTE OF SCIENCE AND TECHNOLOGY**

**I hereby declare that all the information in this study I presented as my Master's Thesis, called "Numerical Analysis of Thermal Performance for Parabolic Trough Solar Collector Using Al<sub>2</sub>O<sub>3</sub> Nano-Fluid" has been presented in accordance with the academic rules and ethical conduct. I also declare and certify on my honor that I have fully cited and referenced all the sources I made use of in this present study.**

**Date 15/ 05/2017**

**Rahell M.R**



## **ACKNOWLEDGEMENTS**

First of all I am grateful to The Almighty Allah for helping me to complete this thesis. I would like to express gratitude to my supervisor, Assist. Prof. Dr. Mohamed Salem Elmnefi, for his patience, encouragement, useful advice, discussion, comments and understanding my situation. He gave me opportunities to present my work in front of experts in the field.

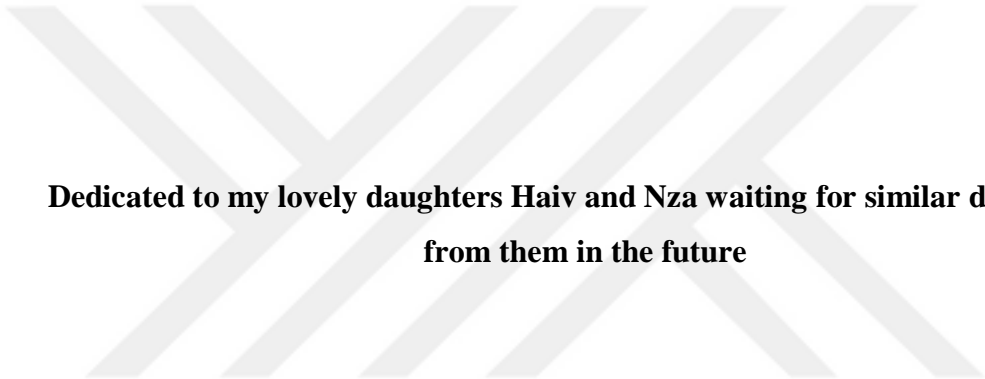
I am forever profoundly indebted to my parents, for their supports, without their prayers the completion of this thesis would not have been possible.

Thanks to my sister, brothers, family and friends.

I would like to express my profound gratitude to my daughters Haiv and Nza, to whom this work is dedicated, for every time they needed me but I wasn't there. For missing me throughout my study.

The most of all my sincere love and infinite appreciation goes to my wife, Huda Mohammed, for being everything in my life, for his patience, supporting, invaluable assistance, for every time she listened to me when reviewing the thesis.

**Rahell M.R**



**Dedicated to my lovely daughters Haiv and Nza waiting for similar dedications  
from them in the future**

## TABLE OF CONTENTS

TABLE OF FIGURE .....	VII
LIST OF TABLE .....	IX
Nomenclature .....	X
ABSTRACT.....	XIII
ÖZET .....	XV
CHAPTER ONE .....	1
INTRODUCTION .....	1
1.1 Introduction .....	1
1.2 Thesis Objective.....	2
1.3 Significance of This Study.....	2
1.4 Organization of the Thesis .....	2
CHAPTER TWO .....	4
SOLAR THERMAL TECHNOLOGY.....	4
2.1 Literature review .....	4
2.2 Main purpose of solar technology.....	6
2.3 Collectors' classification .....	6
1. Output energy from collector.....	6
2. Design and dimensions of collector .....	6
3. Cooling system for collector .....	7
4. Sun tracking method by the collector.....	7
2.4 Idea of concentrating collectors .....	7
2.5 Concentrating Collectors' Categories: .....	7
2.5.1 Parabolic Dish.....	7

2.5.2	Central Receiver System.....	8
2.5.3	Linear Fresnel Reflector.....	9
2.5.4	Parabolic Trough Collector.....	10
2.6	Main component of parabolic trough collector concerned:.....	11
2.6.1	Reflector.....	12
2.6.2	Receiver tube.....	12
2.6.3	Glass Cover tube.....	13
2.6.4	Circulating fluid.....	13
CHAPTER THREE .....		14
NANO-FLUID.....		14
3.1	Nano-fluid properties .....	14
3.1.1	Density of Nano-fluid.....	14
3.1.2	Specific heat of Nano-fluid.....	14
3.1.3	Thermal conductivity of Nano-fluid.....	15
3.1.4	Dynamic Viscosity of Nano-fluid.....	15
3.2	Base fluid properties: .....	15
CHAPTER FOUR.....		17
THEORY.....		17
4.1	Solar thermal analysis .....	17
4.2	Fluid flow analysis inside the receiver tube.....	20
4.3	Receiver tube wall analysis .....	23
4.4	Glass cover temperature.....	25
4.5	Optical and thermal efficiency: .....	27
4.6	Solution time for the code:.....	27
CHAPTER FIVE .....		29



RESULT AND DISCUSSION .....	29
5.1 Fluid Properties .....	29
5.1.1 Specific heat capacity.....	29
5.1.2 Thermal conductivity .....	31
5.1.3 Density .....	32
5.1.4 Dynamic viscosity.....	34
5.1.5 Prandtl number.....	35
5.2 Verification processes steps .....	37
5.2.1 Temperatures distribution along the collector .....	38
5.2.2 Reynold number along the collector .....	39
5.2.3 Nusselt number along the collector.....	40
5.2.4 Heat transfer coefficient.....	42
5.2.5 Heat flux along the collector.....	42
5.2.6 Effect of temperature on heat flux distribution.....	43
5.3 Different fluid inlet temperature.....	44
5.3.1 Effect of fluid inlet temperature on the outlet temperature.....	44
5.3.2 Effect of fluid inlet temperature on the heat gain .....	46
5.3.3 Effect of fluid inlet temperature on thermal efficiency.....	47
5.4 Different solar radiation .....	48
5.4.1 Effect of solar radiation on outlet temperature .....	48
5.4.2 Effect of solar radiation on the heat gain .....	49
5.4.3 Effect of solar radiation on thermal efficiency .....	50
5.5 Various volume flow rate.....	51
5.5.1 Impact of volume flow rate on outlet fluid temperature .....	51
5.5.2 Impact of volume flow rate on heat gain .....	52

5.5.3	Impact of volume flow rate on thermal efficiency and choosing an optimum case.....	53
5.6	Addition of aluminum particles to the base fluid with various volume flow rate.....	54
5.6.1	Effect of nanoparticles on fluid outlet temperature .....	54
5.6.2	Effect of nanoparticles on heat gain with various volume flow rate .....	56
5.6.3	Effect of nanoparticles on thermal efficiency with range of volume flow rate.....	58
5.7	Various range of Reynold number .....	60
5.7.1	Effect of Reynold number fluid outlet temperature with different powder concentration .....	60
5.7.2	Effect of aluminum powder on the useful heat gain with range of Reynold number.....	62
5.7.3	Enhancement investigation of thermal efficiency by powder concentration with a range of Reynold number. ....	63
CHAPTER SIX.....		65
CONCLUSION AND FUTURE WORK .....		65
6.1	Conclusion.....	65
	Future Work .....	66
Appendix (A) .....		67
References.....		68

## TABLE OF FIGURE

Figure 2.1: Parabolic dish collector [4].....	8
Figure 2.2: Central receiver system [4].....	9
Figure 2.3: Linear Fresnal Reflector.....	10
Figure 2.4: Parabolic trough collector [22].....	11
Figure 2.5: Cross sectional scheme of parabolic trough collector.....	12
Figure 2.6: Receiver covered with glass cover [21] .....	13
Figure 4.1: Characteristics of control volume of fluid inside the receiver .....	20
Figure 4.2: Heat transfer numen-culture for solar (PTC) .....	23
Figure 4.3: Characteristics control volume receiver wall .....	24
Figure 4.4: Characteristics control volume receiver wall and glass cover wall for first and last control volume.....	25
Figure 4.5 : Simulations block diagram.....	28
Figure 5.1: Specific heat capacity as a function of temperature and different powder concentration.....	30
Figure 5.2: Specific heat as a function of powder concentration and temperature. ....	30
Figure 5.3: Thermal conductivity as a function of temperature and powder concentration. ....	31
Figure 5.4: Influencing of thermal conductivity by powder concentration at (300 K, 450 K and 600 K).....	32
Figure 5.5: Density as a function of temperature and different powder concentration. ..	33
Figure 5.6: Influencing of density by powder concentration at (300K, 450K and 600K). ....	33
Figure 5.7: Dynamic viscosity as a function of temperature and different powder concentration.....	34
Figure 5.8: Influencing of dynamic viscosity by powder concentration at (300 K, 450 K and 600 K).....	35
Figure 5.9: Prandtl number as a function of temperature and different powder concentration.....	36
Figure 5.10: Influencing of Prandtl number by powder concentration at (300 K, 450 K and 600 K) .....	36

Figure 5.11: Temperatures profile along the collector.....	39
Figure 5.12: Reynold number changing inside receiver tube along the collector .....	40
Figure 5.13: Nusselt number along the collector .....	41
Figure 5.14: Relation between Reynold number and Nusselt number .....	41
Figure 5.15: Heat transfer coefficient inside the receiver tube. ....	42
Figure 5.16: Heat flux along the receiver. ....	43
Figure 5.17: Temperature and heat flux distribution along the collector.....	44
Figure 5.18: Relationship between inlet and outlet fluid temperature.....	45
Figure 5.19: Enlarged section relationship between inlet and outlet fluid temperature..	46
Figure 5.20: Heat gain as a function of fluid inlet temperature. ....	47
Figure 5.21: Thermal efficiency as a function of fluid inlet temperature. ....	48
Figure 5.22: Fluid out let temperature as a function of solar radiation.....	49
Figure 5.23: Heat gain as a function of solar radiation. ....	50
Figure 5.24: Effect of solar radiation in thermal efficiency.....	51
Figure 5.25: Fluid outlet temperature influencing various volume flow rate. ....	52
Figure 5.26: Heat gain influencing various volume flow rate. ....	53
Figure 5.27: Thermal efficiency with various volume flow rate for optimum case. ....	54
Figure 5.28: Fluid outlet temperature as a function of volume flow rate and powder concentration at inlet temperature of (a) 400 K, (b) 500 K, (c) 600 K and (d) 650 K. ....	55
Figure 5.29: Useful heat gain as a function of volume flow rate and powder concentration at inlet temperature of (a) 400 K, (b) 500 K, (c) 600 K and (d) 650 K.....	57
Figure 5.30: enlarged sections of Figure 5.29' for Y-axis only.....	58
Figure 5.31: Thermal efficiency as a function of volume flow rate and powder concentration at inlet temperature of (a) 400 K, (b) 500 K, (c) 600 K and (d) 650 K. ....	59
Figure 5.32: enlarged sections of Figure 5.31' for Y-axis only.....	60
Figure 5.33: Fluid outlet temperature as a function of Reynold number and powder concentration at inlet temperature of (a) 400 K, (b) 500 K, (c) 600 K and (d) 650 K. ....	61
Figure 5.34: Useful heat gain as a function of Reynold number and powder concentration at inlet temperature of (a) 400 K, (b) 500 K, (c) 600 K and (d) 650 K.....	63
Figure 5.35: Thermal efficiency as a function of Reynold number and powder concentration at inlet temperature of (a) 400 K, (b) 500 K, (c) 600 K and (d) 650 K. ....	64

## LIST OF TABLE

Table 1: Aluminum powder properties [31] .....	16
Table 2: PTC specifications and design dimensions used in the model validation (SNLM) from [10] .....	37
Table 3: Experimental data from Sandia National Laboratory compared with numerical analysis.....	38



## Nomenclature

$\phi$	Powder concentration in the base fluid [%]
$\rho$	Density [kg /m <sup>3</sup> ]
$C_p$	Specific heat capacity [J/(kg K)]
$k$	Thermal conductivity [W/(m K)]
$\mu$	Dynamic viscosity [Pa s]
$D_p$	Nanoparticles diameter [nm]
$S_r$	incident solar radiation absorbed per unit area of the receiver [W/m <sup>2</sup> ]
$I_b$	Solar radiation [W/m <sup>2</sup> ]
$\rho_o$	surface reflectivity [dimensionless]
$\tau$	Glass cover transmittance [dimensionless]
$\alpha$	Absorptance [dimensionless]
$\gamma$	Shape factor [dimensionless]
$F_a$	incident angle modifier [dimensionless]
$C$	Collector's Concentration ratio [dimensionless]
$\dot{q}_u$	Heat flux on outer surface of receiver to inside [W/ m <sup>2</sup> ]
$\dot{q}_{loss}$	Heat flux to ambient [W/ m <sup>2</sup> ]
$h_{conv,r-amb}$	Convective heat transfer coefficient between receiver and ambient [W/(m <sup>2</sup> K)]
$h_{rad,r-sky}$	Radiative heat transfer coefficient between receiver and sky [W/(m <sup>2</sup> K)]
$h_{conv,r-c}$	Convective heat transfer coefficient between receiver and cover [W/(m <sup>2</sup> K)]
$h_{rad,r-c}$	Radiative heat transfer coefficient between receiver and cover [W/(m <sup>2</sup> K)]
$T_r$	Receiver temperature [K]
$T_{amb}$	Ambient temperature [K]

$T_{sky}$	Sky temperature [K]
$T_c$	Glass cover temperature [K]
$T_{anul}$	Receiver and glass cover Annuals temperature [K]
$T_f$	Fluid mean temperature [K]
Ra	Rayleigh number [dimensionless]
Pr	Prandtl number [dimensionless]
$D_{c,ext}$	Cover external diameter [m]
$D_{c,in}$	Cover internal diameter [m]
$D_{r,ext}$	Receiver external diameter [m]
$D_{r,int}$	Receiver internal diameter [m]
$\sigma$	Steven Boltzmann constant [ $5.6697 \times 10^{-8} \text{ W}/(\text{m}^2 \text{ K}^4)$ ]
$\varepsilon_r$	Receiver emittance [dimensionless]
$\varepsilon_c$	Glass cover emittance [dimensionless]
$F_{rc}$	View factor between receiver and cover [dimensionless]
g	Gravitational acceleration [ $\text{m}/\text{s}^2$ ]
$\beta$	Thermal expansion [ $1/\text{K}$ ]
$\dot{q}_{wall}$	Heat flux from receiver inner surface to the fluid [ $\text{W}/\text{m}^2$ ]
$\Delta z$	Length of control volume [m]
$\dot{m}$	Mass flow rate [kg /s]
$A_f$	Cross section area of fluid flowing [ $\text{m}^2$ ]
$\Delta t$	Time [s]
$\bar{\rho}$	Density at center of control volume at time step (for transient state) [ $\text{kg} /\text{m}^3$ ]
$\bar{\rho}^o$	Density at center of control volume at previous time step [ $\text{kg} /\text{m}^3$ ]
$\dot{V}$	Volume flow rate [l/min]
$u$	Velocity [m /s]
Re	Reynold number [dimensionless]
Nu	Nusslt number [dimensionless]

$h_f$	Convective heat coefficient inside receiver tube [W/(m <sup>2</sup> K)]
$\eta_{op}$	Optical efficiency [dimensionless]
$\eta_{th}$	Thermal efficiency [dimensionless]
$\dot{Q}_u$	Useful energy gain [W]
$A_{ref}$	Reflector's area [m <sup>2</sup> ]





# **ABSTRACT**

## **NUMERICAL ANALYSIS OF THERMAL PERFORMANCE FOR PARABOLIC TROUGH SOLAR COLLECTOR USING $\text{Al}_2\text{O}_3$ NANO-FLUID**

M.R, Rahell

Master, Department of Mechanical and Aeronautical Engineering

Thesis supervisor: Assist. Prof. Dr. Mohamed Salem ELMNEFI

May –2017, 72 page

Due to the necessity of live and rapidly growing in population, energy providing have been a big problem for many countries. Solar energy has less economic and environmental barriers for energy providing by the governments. This reason have been encouraging researchers to concern about solar energy as a renewable energy. Solar thermal collectors become the basic part in power plants for power production. Researchers have been interesting in parabolic trough solar collectors as they detect that it could give the best performance among the other types as they worked experimentally and numerically on it. In the current study, the investigation of improving thermal efficiency for solar parabolic trough collector has been carried out by using finite volume method at steady state condition. Firstly, a confirmation procedure have compared the numerical and experimental results. Then the effect of various solar radiation, different fluid inlet temperature and range of volume flow rate on the fluid out let temperature, useful heat gain and thermal efficiency have been analyzed. Finally, aluminum powder have added to the base fluid in order to obtain Nano-fluid. Various volume flow rate and different range of Reynold number applied with using Nano-fluid. Calculations with Nano-fluid made at three different volumetric concentration of nanoparticles (1%, 4% and

8%) at the same condition of verification. this study provides important keys to collectors manufacturers and solar power plants in selecting suitable operation condition so that the performance is maximum.

**Keywords:** Solar Collector, Nano-fluid, Finite Volume Method, Thermal Efficiency.



## ÖZET

### AL<sub>2</sub>O<sub>3</sub> NANO- AKIŞKAN KULLANILARAK PARABOLİK TRAF GÜNEŞ KOLEKTÖR İÇİN TERMAL PERFORMANSIN SAYISAL ANALİZİ

M.R, Rahell

Yüksek lisans, Makine ve Uçak Mühendisliği Bölümü

Tez Danışmanı, Yardımcı Doç. Dr. Mohamed Salem ELMNEFI

Mayıs - 2017, 72 sayfa

Hızlı Nüfus artışı, nedeniyle enerji ihtiyacı sağlayan pek çok ülke için büyük bir sorun olmuştur. Güneş enerjisinin, hükümetler tarafından sağlanan enerji için daha ekonomik ve az çevresel engelleri vardır. Bu nedenle, araştırmacıları güneş enerjisini yenilenebilir bir enerji olarak düşünmeye teşvik ediyorlardı. Güneş enerjisiyle çalışan termal toplayıcılar, enerji üretiminde kullanılan santrallerin temel parçası haline gelir. Deneysel ve sayısal olarak üzerinde çalışıldığından, araştırmacılar parabolik traf güneş kolektörlerinde ilginçti çünkü diğer türler arasında en iyi performansı verebileceklerini tespit ettiler. Bu çalışmada, parabolik traf güneş kolektörler oluk toplayıcı için termal verimliliğin geliştirilmesi araştırması, sabit hal koşullarında sonlu hacim yöntemi kullanılarak gerçekleştirilmiştir. Öncelikle, bir onay prosedürü sayısal ve deneysel sonuçları karşılaştırdı. Sonra, çeşitli güneş radyasyonunun, farklı sıvı giriş sıcaklığının ve hacim akış hızı aralığının akışkanın üzerindeki etkisi, sıcaklığın, faydalı ısı kazanımının ve termal verimliliğin analiz edilmesine izin verir. Nano sıvı elde etmek için sonunda alüminyum tozu baz sıvısına ilave edilmiştir. Çeşitli hacim akış hızı ve Nano-sıvı kullanılarak uygulanan farklı Reynold sayısı aralığı, Nano-akışkan ile yapılan hesaplamalar, aynı doğrulama koşulu altında üç farklı hacimsel nanopartikül konsantrasyonunda (% 1, % 4 ve % 8) yapılır. Bu çalışma kolektör üreticilerine ve güneş

enerjisi santrallerine, uygun çalışma koşullarının seçilmesinde, performansın maksimum olması için önemli anahtarlar sağlar.

**Anahtar Kelimeler:** Güneş Kolektörü, Nano-akışkan, Sonlu Hacim Yöntemi, Isıl Verimlilik.



# CHAPTER ONE

## INTRODUCTION

### 1.1 Introduction

Energy consumption have been increasing recently as a requirement of life. The significantly growing of population leads to that. According to the Word Energy Outlook in (2012), energy request is expected to be increased about double for the period 2012 until 2035. Till now, Fossil fuel is prevailing between other fuels sources for total energy supply in the world. According to the Outlook of International Energy, 84.5% of the global energy consumed is delivered by fossil fuels [1]. Too many problems caused by by-products of fossil fuels. Such as releasing of carbon dioxide which is the main source that resulting global warming. On the other hand, the unsuitability of fossil fuels price is another problem for poor countries. These environmental and economic impacts results to think about alternative sources cheap and environmentally friendly. These points make governments and companies to concern about renewable energy like wind, and solar energy [2].

Solar thermal technology by parabolic trough collector for energy producing become the most popular among the other types of solar collectors. Thermal conversion process for solar parabolic trough collector (PTC) may be divided into the following fragments. The irradiance from solar is collected by the parabolic trough collector, then redirected and focused to the external surface of the absorber tube where the energy of radiation is changed to thermal energy. Thermal energy will transfer to the internal surface of the absorber tube by conduction. Finally, this energy will be removed by the heat transfer fluid (HTF) which is continuously flowing inside the absorber tube by force convective heat transfer [3-5].

Experimental studies have been done in order to improve the performance of parabolic trough solar collector by using different heat transfer fluids [6]. Also solar (PTC)

have been simulated numerically by using finite different method, finite volume method, and using finite element method in commercial software like Solid work with using different working fluid with nano-particles [7-9].

## **1.2 Thesis Objective**

The main goal of this thesis is to prove that the parabolic trough solar collector performance can be improved by the use of Nano-fluid at steady state condition and thesis objective are as follows:

1. Study the influence of thermal efficiency by solar radiation, fluid inlet temperature and volume flow rate with nano-fluid.
2. Using finite volume method in the simulation procedure by coding in Matlab.
3. Present the effect of nanoparticles addition in the improving of parabolic trough collector's performance.

## **1.3 Significance of This Study**

This study will present a numerical modeling for estimating parabolic trough solar collectors' thermal efficiency in the steady state condition. In addition to its significance to researchers concerned in the field, this research provides important keys to parabolic trough solar collectors' power plants in selecting the operation condition and powders ratio in the base fluid so that better performance can be obtained.

## **1.4 Organization of the Thesis**

Chapter one: at first, this chapter is introduces a general overview of the topic then presenting summary of previous studies that concerned with parabolic trough solar collector after that objective and significant of this study have explained and finally its organization.

Chapter 2: A brief descriptions of numerical simulations and experimental studies that carried out in the previous researches. In addition of the main purpose of solar thermal technology, classification of solar thermal collectors and main component of parabolic trough collector.

Chapter 3: Discusses properties of Nano-fluid such as specific heat, density, thermal conductivity and dynamic viscosity. In addition of base fluid's properties.

Chapter 4: Presenting the methodology of simulation for solar thermal analysis then fluid flow analysis inside receiver tube after that axial temperature distribution in receiver tube and glass cover. Finally, thermal efficiency for parabolic trough solar collector.

Chapter 5: showing the simulation results for verification procedure, effect of solar radiation, fluid inlet temperature and volume flow rate on the thermal efficiency. Finally, the impact of aluminum powder ( $\text{Al}_2\text{O}_3$ ) with using different powder ratio as a function of volume flow rate on thermal efficiency.

Chapter 6: Conclusion of the thesis, and highlighting for the future work.

## **CHAPTER TWO**

### **SOLAR THERMAL TECHNOLOGY**

#### **2.1 Literature review**

Engineering design of collectors requires simulation. It has taken to reach the best design and operating conditions in order to reach the highest performance as possible. The analysis have been including concentrator, receiver tube and working fluid. The previous studies have been done in the different ways.

Numerical model by using finite volume method (FVM) has carefully validated with experimentally recorded data taken from Sandia National Laboratories. Numerical simulation in detail estimated for thermal and fluid dynamic manners of a single-pass parabolic trough collector is carried out. The model is extended to include double pass circulating of HTF. A visible improving have seen in thermal efficiency by the use of counter flow concentric circular heat exchangers (double-pass)[10].

In a hot climate of Algerian Sahara one-dimensional simulation have done by developing the computer program which based on implicit finite difference method (FDM) with energy balance approach. Liquid water and liquid TherminolVP-1™ synthetic oil. The simulation results that the thermal efficiency decline in high temperature of TherminolVP-1™ and rises by 2% in the low water temperature[11].

Computational fluid dynamics (CFD) tools have used in order to analyze the impact of internally finned tubes on heat transfer phenomena, thermo-mechanical stress and thermal weariness and pressure losses. In the same condition, they have proposed that a



set of helically finned tube improved thermal efficiency of collector by 3% in a comparing with a reference commercial tube[2].

The enhancement of heat transfer in the receiver tube of solar (PTC) has investigated by porous inserting inside the tube with non-uniform heat flux condition. A new optimization technique has been coupling genetic algorithm and computational fluid dynamics in order to propose the optimum porous insert configuration. The results presented that the heat transfer performance investigated by porosity of porous, its thermal conductivity, and Reynold number[12].

Enhancement of Nusselt number has been investigated by using two segmental rings inside receiver tube. The numerical simulation applied for a constant distance between the rings. It has shown from the result the enhancement in Nusselt number increase with decreasing inner diameter of segmental rings[13].

Another simulation has done for receiver tube is analyzing by Solid Work which is a commercial software based on the finite elements method. A small model of solar (PTC) is designed and simulated for various operating conditions. The aim the study was to estimate the efficiency of the model and for analyzation of heat transfer phenomena which occur inside the receiver, heat flux and temperature distribution in the receiver wall. The final results demonstrated that the (PTC) has model performed efficiently, in addition all calculations are validated[14].

Engineering Equation Solver (EES) have been used for energetic and exergetic analysis of solar (PTC). Seven different fluid utilized for a wide range of temperature (300K-1300K) each fluid in its possible range. It has proved if gas is worked as a heat transfer fluid the performance will be lower than the operating by liquid working fluid in the optimum mass flow rate of each fluid[6].

Performance investigation of a parabolic solar collector in an experimental study has conducted water base Nano-fluid ( $\text{SiO}_2\text{-H}_2\text{O}$ ). Different volumetric concentration ratio (0.01% and 0.05%) have been used in the testing for Nano-fluid preparation. Sunlight tracking was manually in the experimentation during the day long. It has been observed from the results that ( $\text{SiO}_2\text{-H}_2\text{O}$ ) base Nano-fluid has relatively higher thermal efficiency at higher flow rates[15].

The second law of thermodynamic in receiver tube which is entropy generation and thermal efficiency of the parabolic trough collector have been reported at a different range of geometric concentration ratio (88-113). Computational of fluid dynamic (CFD) procedure was carry out in order to obtain the numerical solution of the thermal efficiency and thermodynamic performance for the system. At a given flow rate, thermal efficiency became less by about 4.5% when the concentration ratio grows from 88 to 113 whereas the rate of entropy generation is shown to be increased with the increasing of concentration ratio. The result also indicates that heat transfer enhancement occurs by the use of Cu-TherminolVP-1 Nano-fluid as working fluid. The thermal efficiency growths by about 12% as the powder volume fraction rises from (0% to 6%)[8].

## **2.2 Main purpose of solar technology**

Energy consumption has become one of the major problems in the world, due to population growth and the requirement of life for energy. The continuous researches have been done for an alternative power source as result of the instability of fossil fuels price and its environmental impact. The development of solar energy as an alternative source of power in last three decades is reached a remarkable edge. The main point in the studies were solar collectors [8, 9].

## **2.3 Collectors' classification**

Solar Collectors have been classified in different ways. According to the previous studies, the classification have done in to three main categories [4, 16, 17]

### **1. Output energy from collector**

- Solar thermal collectors
- Solar photovoltaic collectors
- Solar photovoltaic /thermal hybrid collectors (hybrid system)

### **2. Design and dimensions of collector**

- Flat plate collectors

- Concentrating collectors
- Compound Parabolic Concentrator

### **3. Cooling system for collector**

- Cooling by natural convection
- Cooling by forced convection

### **4. Sun tracking method by the collector**

- Movable with the sun in one or two axis
- Fixed during day long

## **2.4 Idea of concentrating collectors**

The concentrating collector is a type collector which provide energy at higher temperatures than that of flat plate collectors. Concentrating collectors re-direct solar radiation by an aperture into a thermal absorber and usually needs tracking of the sun in one or two axes. In this type of collectors, solar energy is optically focused before being transferred to heat. Concentration process of solar radiation can be obtained by reflection or refraction of radiance by using mirrors or lens. Concentrating collectors may also be classified to imaging and non-imaging depending on that the image of the sun is focusing at the receiver or not. All types of concentrating collectors belong to the imaging type. The main types of the concentrating collectors are presenting next [4, 18].

## **2.5 Concentrating Collectors' Categories:**

### **2.5.1 Parabolic Dish**

Parabolic dish concentrator, as shown schematically in Figure 2.1'. It is a point-directing collector. It is focusing solar radiation onto a receiver positioned at dishes focal point, it can track the sun in two axes. The dish structure should track fully the sun in order to redirect the sunbeam into the thermal receiver. Parabolic-dish systems may reach temperatures more than 1500 °C. Because of that the receiver is distributed throughout collector field that is why this type defined as distributed-receiver systems. The concentrated sunbeam absorbed by individual receivers and deliver this power through a heat-transfer fluid to the power conversion system for generating electricity[4].

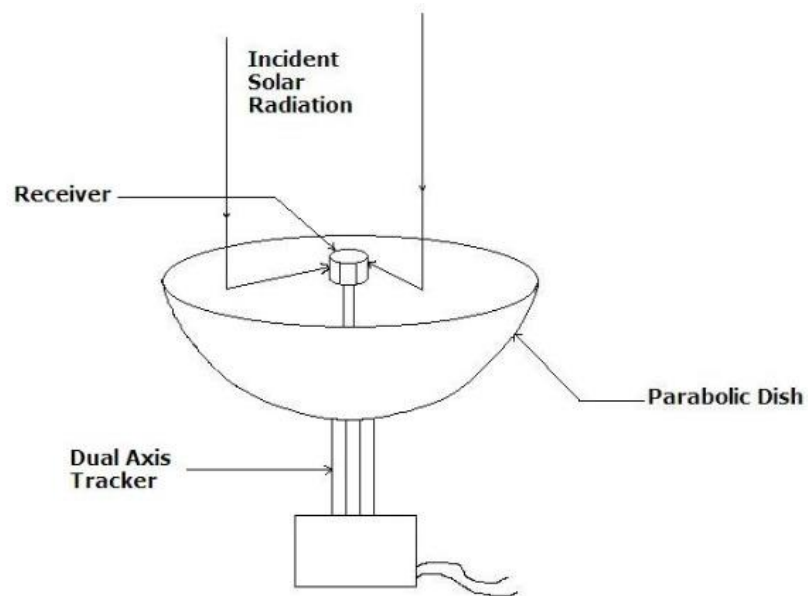


**Figure 2.1:** Parabolic dish collector [4]

### **2.5.2 Central Receiver System**

There are three main configurations for the solar collector with receiver systems (Figure 2.2'). In the first, heliostats completely surround the receiver tower for obtaining extremely high inputs of solar radiation, a multiplicity of reflectors, using altazimuth amount of mirror can be used to re-direct solar irradiance onto a common target. In second is a receiver, which is cylindrical usually puts on the top of the tower. It has an exterior heat transfer surface. In addition of heat transfer fluid which absorbs energy from the receiver and delivers it to the extern system in order to generate steam subsequently generate electricity in steam power plant[19].

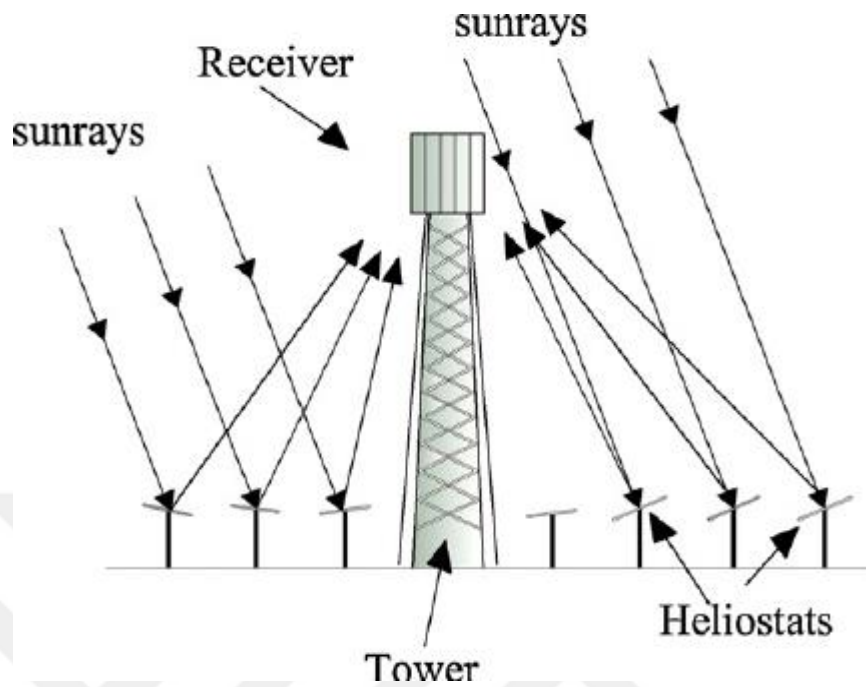


**Figure 2.2:** Central receiver system [4]

### 2.5.3 Linear Fresnel Reflector

Linear Fresnel Reflector (LFR) composed of receiver and reflector. The receiver tube is fixed in the space above the reflector field as shown in (Figure 2.3'). The reflector is consist of many low row parts. Reflector rows focus together on an elevated long receiver tube, which running parallel with the reflector rotational axis. This system offering a lower cost solution when the absorber row is sharing among several rows of reflectors[4, 20].

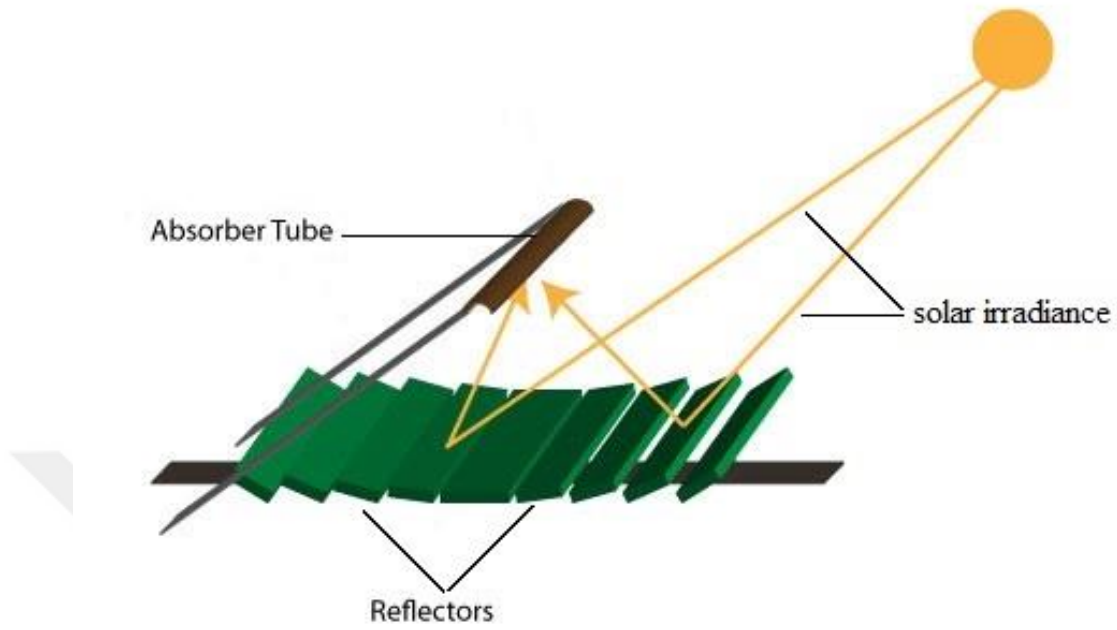


**Figure 2.3:** Linear Fresnel Reflector

#### 2.5.4 Parabolic Trough Collector

Solar parabolic trough collector is focusing solar irradiance by a parabolic shape reflector onto a receiver tube (Figure 2.4'). The reflected sunbeam has absorbed by the receiver. The collected energy in the tube wall is absorbing by a working fluid. The absorbed heat by fluid generally used to generate steam in order produce electricity in the power plants. The main deference of parabolic trough collector (PTC) with Linear Fresnel reflector is that in the solar (PTC) the receiver fixed with a parabolic reflector and moving with it during beam tracing. But in (LFR) the receiver is fixing on the tower and each reflector row moving separately according to its location to the receiver tube[5, 21].

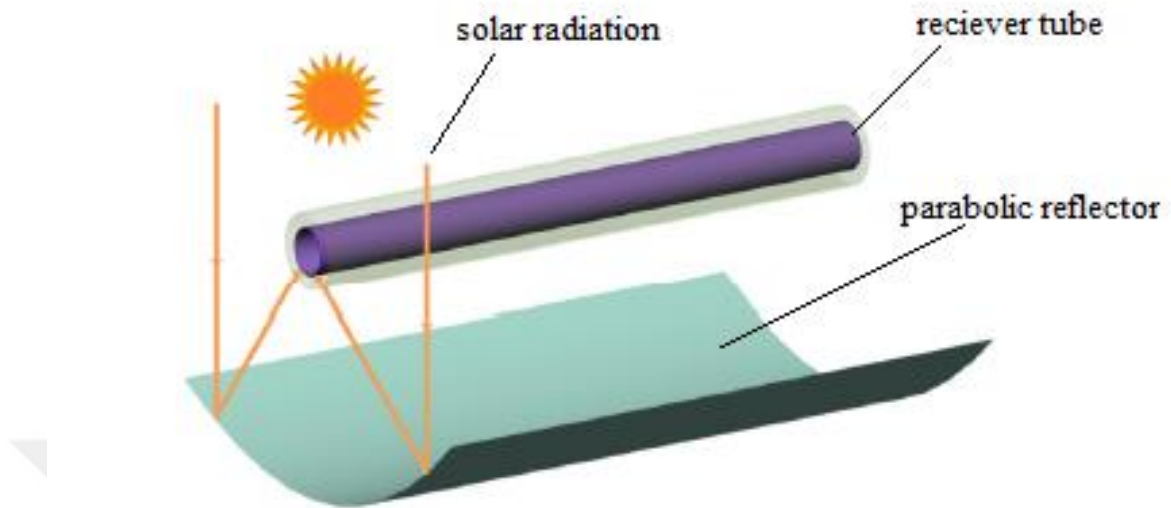


**Figure 2.4:** Parabolic trough collector [22]

## **2.6 Main component of parabolic trough collector concerned:**

This section is explaining the components of solar (PTC) and their main properties and applications. As described in the previous section, solar PTC is a focal line solar concentrating collector where thermal fluid flows through a receiver tube in order to absorb the concentrated energy of solar radiation redirected by parabolic trough-shaped mirrors. Solar (PTC)s applications may be divided into two major groups depending on the range of temperature. The first and the most important application for electric generation by the solar concentrated power plants (SCPP) where temperature range are from 300 to 400 °C. The second group of the applications requires lower temperature than first type which is between 100 and 250 °C. The most important uses of the second temperature range are in the industrial process heat (IPH), space heating, low-temperature heat requirement, swimming pool and refrigeration and cooling system. There are two techniques for solar PTC integration field. Directly generating steam from the solar(PTC) by using (Direct Steam Generation technology) or indirectly, by heating heat transfer fluid(HTF) in the solar field and using it for steam generate in a heat exchanger where called (Heat Transfer Fluid (HTF) technology)[6, 21].

### 2.6.1 Reflector

This part is one of the main part of parabolic trough solar collector which the other main parts influences it during sun tracing. It's usually made by bending a very reflective metallic sheet with the lowest absorptivity in to a parabolic shape. In the most designs, it tracing sunbeam by rotating in an axis which is the north-south horizontal focal axis. The incident sunlight coming parallelly from the sun onto the reflector and it concentrate it in focal line (Figure 2.5')[23].

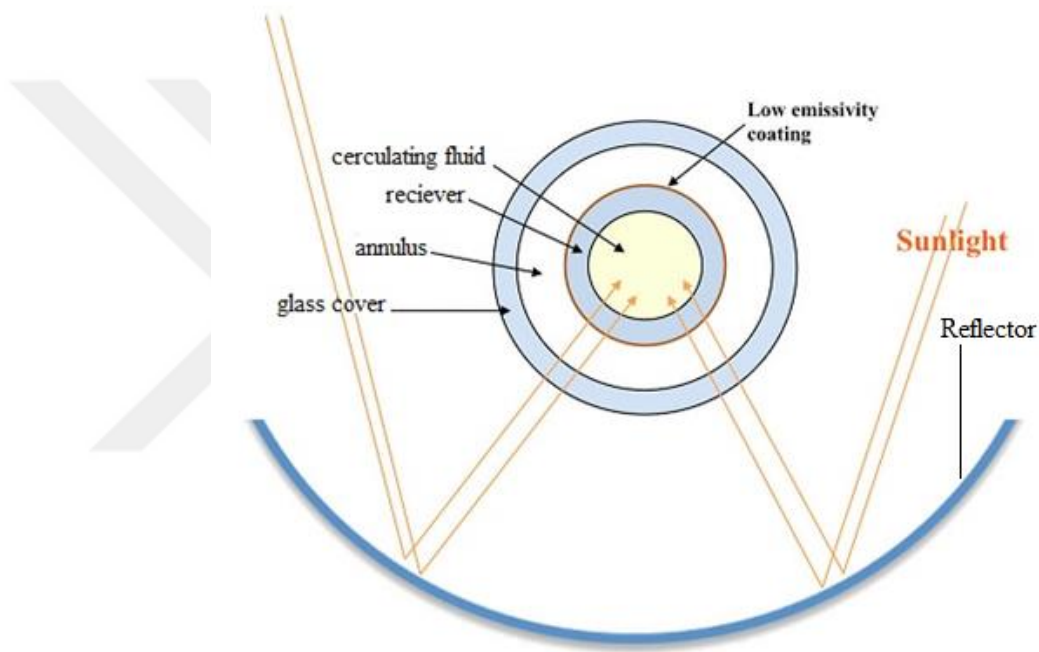


**Figure 2.5:** Cross sectional scheme of parabolic trough collector

### 2.6.2 Receiver tube

The collected energy by the concentrator in the focal line absorbed by the absorber tube which placed in the focal point as shown in (Figure 2.4'). The receiver tube always made from stainless steel. The multilayer of metal ceramic has been using to cote the steel tube in order to obtain the highest absorptivity for solar radiation and to provide lowest thermal emissivity as possible(Figure 2.5'). Consequently, they lead to reduce thermal loss during the operation and exactly at high temperature[24].



### 2.6.3 Glass Cover tube

The receiver metallic tube is enclosed with glass envelop to provide the reduction of heat loss by convection and radiation from its outer surface. The annulus between the receiver and glass cover has evacuated from the air in order to significantly reduce thermal losses at the high operating temperature which occurs by convection and to protect the outer surface of the absorber tube from oxidation. The cylindrical glass cover has an outer antireflective coating to decrease Fresnel reflective losses from external glass surface and maximizing the solar transmittance (Figure 2.6') [21, 25].

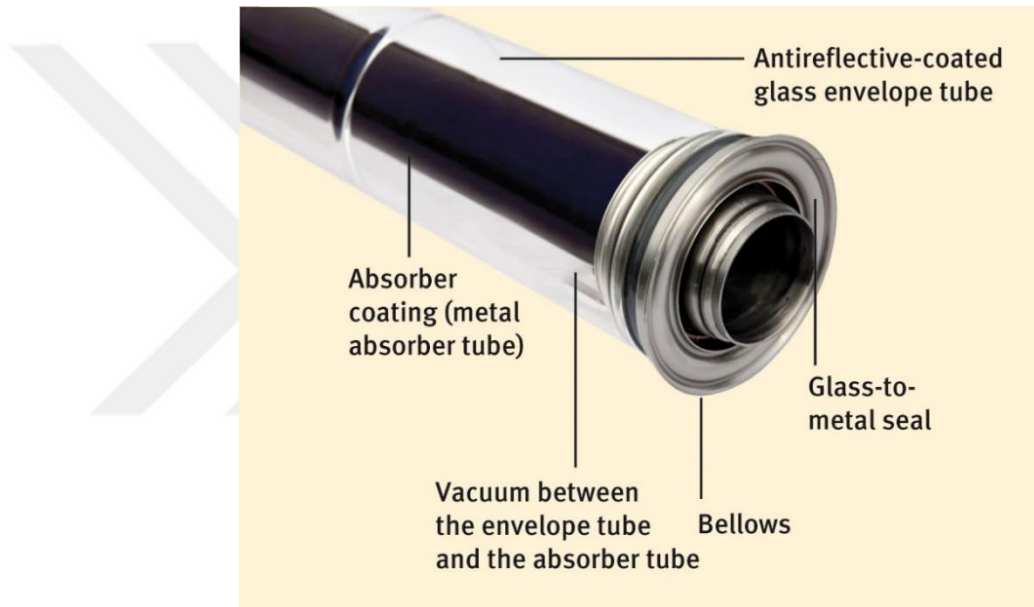


**Figure 2.6:** Receiver covered with glass cover [21]

### 2.6.4 Circulating fluid

The energy collected in the receiver tube wall is derived out by fluid which defined as a heat transfer fluid (HTF). Circulating heat transfer fluid in the receiver tube bringing solar thermal energy to the power unit all day long. Heat transfer fluid selection can affect the thermal efficiency of solar parabolic trough collector that may be used in power plant. Several kinds of (HTF) are able to use in solar (PTC) plants. Thermal oils have been utilized commonly like heat transfer fluid in solar (PTC) Plants because it has not produced high pressure inside the receiver tube in a comparable with water. The stability, safety and the requirement of environmental protection be able to satisfy with reasonable effort [26-28].

## CHAPTER THREE

### NANO-FLUID

#### 3.1 Nano-fluid properties

More accurate result for numerical simulation depends on the Thermo-physical properties of used working fluid. Synthetic oil has been used with nanoparticles in order to produce Nano-fluid. Synthetic oil strongly depends on temperature. Its properties can be calculated at any temperature and also it can improve more by mixing nanoparticles with it. In the current work, (  $\text{Al}_2\text{O}_3$  ) as a nanoparticles mixed with base fluid because it has suitable Thermophysical properties. The Nano-fluid properties (density, dynamic viscosity, heat capacity in a constant presser and thermal conductivity) are estimated by the following formulas:

##### 3.1.1 Density of Nano-fluid

Density was calculated by Pak and Choi's correlation which is usual formula settled for conventional solid-liquid mixture [25, 29, 30]:

$$\rho_{nf} = (1 - \phi) \rho_b + \phi \rho_p \quad 3.1$$

##### 3.1.2 Specific heat of Nano-fluid

Specific heat capacity have been estimated by supposing thermal equilibrium in the nano-fluid between aluminum particles and oil in the surrounding which calculated by [9, 15]:

$$Cp_{nf} = \frac{(1 - \phi) Cp_b \rho_b + \phi Cp_p \rho_p}{(1 - \phi) \rho_b + \phi \rho_p} \quad 3.2$$

### 3.1.3 Thermal conductivity of Nano-fluid

Bruggeman model have used for thermal conductivity calculation since it gives the most reasonable results with a wide range powders concentration [9, 31]:

$$k_{nf} = 0.25 \left[ (3\phi - 1)k_p + (2 - 3\phi)k_b + \sqrt{\Delta_{nf}} \right] \quad 3.3$$

Where

$$\Delta_{nf} = \left[ (3\phi - 1)k_p + (2 - 3\phi)k_b \right]^2 + 8k_p k_b \quad 3.4$$

### 3.1.4 Dynamic Viscosity of Nano-fluid

Maiga empirical correlation is considered for dynamic viscosity calculation. This formula have gotten from least square-curve fitting experimental data [9, 32]:

$$\mu_{nf} = \mu_b (123\phi^2 + 7.3\phi + 1) \quad 3.5$$

Where  $\phi$  = powders concentration in the base fluid

## 3.2 Base fluid properties:

For base fluid, curve-fitted polynomials which strongly depends on temperature taken from the manufactured data sheet. The density ( $\rho_b$ ) in ( $kg / m^3$ ), the specific heat capacity ( $Cp_b$ ) in ( $kJ / kgK$ ) and the thermal conductivity ( $k_b$ ) in ( $W / mK$ ) are defined by the polynomials in the next three formulas respectively [9].

For  $233.15 \leq T \leq 673.15$  K:

$$\rho_b = 1.2691 \times 10^3 - 1.52115 \times T + 1.79133 \times 10^{-3} \times T^2 - 1.67145 \times 10^{-6} \times T^3 \quad 3.6$$

$$Cp_b = 1.10787 + 1.7076 \times 10^{-3} T \quad 3.7$$

$$k_b = 1.90134 \times 10^{-1} - 1.88053 \times 10^{-4} \times T \quad 3.8$$

The dynamic viscosity for synthetic oil ( $\mu_b$ ) in (Pa s) is described by two polynomials for two different range of temperature:

For  $233.15 \leq T \leq 343$  K:

$$\mu_b = (5.14887 \times 10^4 - 9.61656 \times 10^2 \times T + 7.50207 \times T^2 - 3.12468 \times 10^{-2} \times T^3 + 7.32194 \times 10^{-5} \times T^4 - 9.14636 \times 10^{-8} \times T^5 + 4.75624 \times 10^{-11} \times T^6) \times 10^{-3} \quad 3.9$$

For  $343 \leq T \leq 673.15$  K:

$$\mu_b = (9.88562 \times 10^1 - 7.30924 \times 10^{-1} \times T + 2.21917 \times 10^{-3} \times T^2 - 3.42377 \times 10^{-6} \times T^3 + 2.66836 \times 10^{-9} \times T^4 - 8.37194 \times 10^{-13} \times T^5) \times 10^{-3} \quad 3.10$$

**Table 1:** Aluminum powder properties [31]

$D_p/nm$	$k_p/W m^{-1} K^{-1}$	$Cp_p/J kg^{-1} K^{-1}$	$\rho_p/kg m^{-3}$
30	36	773	3880

## CHAPTER FOUR

### THEORY

#### 4.1 Solar thermal analysis

The incident solar radiation absorbed per unit area of the receiver tube for a solar PTC is calculated by equation (4.1) [10, 33]:

$$S_r = I_b \rho_o \tau \alpha \gamma F_a \quad 4.1$$

Glass cover transmittance ( $\tau$ ) has been equaling to one in the absence of cover since it is related to the glass cover.

The useful heat gain per unit of the area for receiver ( $\dot{q}_u$ ) (expressed in terms of the local receiver tube temperature ( $T_r$ ), local cover temperature ( $T_c$ ) and the absorbed incident solar radiation per unit of area by the receiver ( $S_r$ )). Is given by Duffie and Beckman in the following formula:

$$\dot{q}_u = CS_r - \dot{q}_{loss} \quad 4.2$$

Heat loss from non-covered case calculates by equation (4.3) between the receiver and ambient [10, 34]:

$$\dot{q}_{loss} = h_{conv,r-amb} (T_r - T_{amb}) + h_{rad,r-sky} (T_r - T_{sky}) \quad 4.3$$

Where Churchill and Chu's correlation for natural convection around cylinders in the absence of wind have been used in order to estimate ( $h_{conv,r-amb}$ ) in equation (4.4)[10]. And ( $h_{rad,r-sky}$ ) may be assumed as a case of radiation between the surfaces and the sky in equation (4.5)[34].

$$h_{conv,r-amb} = \left[ 0.6 + 0.387 \left( \frac{Ra}{\left( 1 + \left( \frac{0.559}{Pr} \right)^{9/16} \right)^{16/9}} \right)^{1/6} \right]^2 \frac{k_{air}}{D_{c,ext}} \quad 4.4$$

$$h_{rad,r-sky} = \varepsilon_r \sigma (T_{sky}^2 + T_r^2) (T_{sky} + T_r) \quad 4.5$$

Heat loss for non-evacuated (air between receiver and cover) case calculates by:

$$\dot{q}_{loss} = (h_{conv,r-c} + h_{rad,r-c}) (T_r - T_c) \quad 4.6$$

The radiative heat transfer coefficient between the receiver tube and cover is shown by Duffie and Beckman (with considering the view factor in the annulus is 1) in the following formula[10]:

$$h_{rad,r-c} = \frac{\sigma (T_r^2 + T_c^2) (T_r + T_c)}{\frac{(1 - \varepsilon_r)}{\varepsilon_r} + \frac{1}{F_{rc}} + \frac{(1 - \varepsilon_c) D_{r,ext}}{\varepsilon_c D_{r,int}}} \quad 4.7$$

For evacuated tubular cover convective heat transfer coefficient  $h_{conv,r-c}$  between receiver and glass cover considered to be zero. But natural heat transfer convection in the non-

evacuated annular space a horizontal concentric cylinders may define by using the following correlations[10]:

$$k_{eff} = 0.317k_{air} (Ra^*)^{1/4} \quad 4.8$$

Where

$$(Ra^*)^{1/4} = \left[ \frac{\ln\left(\frac{D_{c,int}}{D_{r,ext}}\right)}{b^{3/4} \left( \frac{1}{D_{r,ext}^{3/5}} + \frac{1}{D_{c,int}^{3/5}} \right)^{5/4}} \right] (Ra)^{1/4} \quad 4.9$$

In which hydraulic diameter

$$b = (D_{c,int} - D_{r,int})/2 \quad 4.10$$

The Rayleigh number is

$$Ra = \frac{g\beta(T_r - T_{anul})b^3 Pr}{\nu^2} \quad 4.11$$

The Rayleigh number (Ra), depends on different in temperature in the annular gap and the characteristic length b. in addition to air properties which is taken from appendix (A). The heat transfer coefficient  $h_{conv,r-c}$  is connected with effective thermal conductivity,  $k_{eff}$  and calculated by:

$$h_{conv,r-c} = \frac{2k_{eff}}{D_{r,ext} \ln\left(\frac{D_{c,int}}{D_{r,ext}}\right)} \quad 4.12$$

## 4.2 Fluid flow analysis inside the receiver tube

Since the receiver tube exposed to uniform concentrated solar radiation Fluid flow in the receiver can analyze by assuming the uniform surface heat flux along the receiver tube so for every control volume can be taken as uniform surface heat flux and equation (4.13) can be applied[35]:

$$T_{f,j+1} = T_{f,j} + \frac{\pi \dot{q}_{wall} \Delta z}{\dot{m}_j C p_{f,j}} \quad 4.13$$

Mean fluid temperature at center of control volume:

$$\bar{T}_{f,j} = \frac{T_{f,j} + T_{f,j+1}}{2} \quad 4.14$$

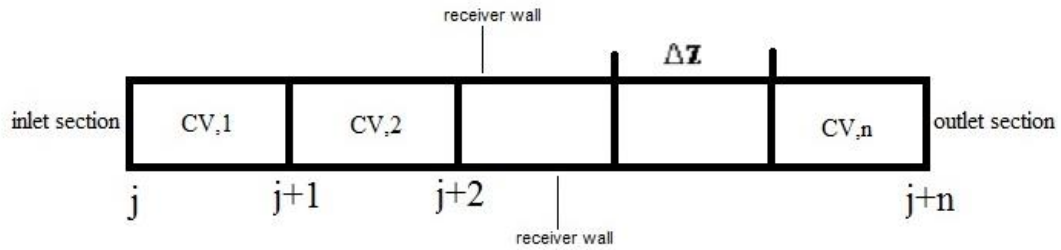


**Figure 4.1:** Characteristics of control volume of fluid inside the receiver

The numerical analysis is implemented in terms of CV method. The equations are discretized and coupled by applying fully implicated step by step method in flowing direction. From the identified values at the inlet of receiver tube and its wall boundary conditions, the unknown values at the outlet of each control volume are iteratively gotten from the continuity equation in the governing form which discretized before by O.García-Valladares and N. Velázquez [10]. Outlet values for each CV become the value of inlet for the next CV. This procedure is continued until the out let of the receiver tube. For each CV, algebraic equations of mass flow rate are produced by a discretization of the continuity equations in order to find the dependent variables values of the mass flow rate at each



control volumes outlet section. Continuity equation had obtained for transient two-phase flow, steady two-phase flow and steady single-phase flow[10].

$$\dot{m}_{j+1} = \dot{m}_j - \frac{A_i \Delta z}{\Delta t} (\bar{\rho} - \bar{\rho}^o) \quad 4.15$$

Since the current study is in compressible flow, one phase and steady state case, each term which contains time term neglects so the equation becomes:

Continuity equation

$$\dot{m}_{j+1} = \dot{m}_j \quad 4.16$$

Volume flow rate could be fined from mass flow rate:

$$\dot{V}_j = \dot{m}_j / \rho_j \quad 4.17$$

Mean Velocity at each cross section can be calculated by:

$$u_j = \dot{m}_j / \rho_j A_i \quad 4.18$$

Reynold number at each cross section estimated by:

$$\text{Re}_j = \rho_j u_j D_{r,\text{int}} / \mu_j \quad 4.19$$

Prenndl number may be defined at any cross section by:

$$\text{Pr}_j = \mu_j C p_j / k_j \quad 4.20$$

Nusslt number

For laminar flow case where  $\text{Re} > 2300$  and uniform surface heat flux equation (4.21) used for Nusslt number estimation[33]:

$$Nu_{lam} = \left( 4.354^3 + 0.6^3 + \left( 1.953 (\text{Re Pr } dr_{in})^{1/3} - 0.6 \right)^3 + \left( 0.924 \text{Pr}^{1/3} \sqrt{\text{Re Pr } dr_{in}} \right)^3 \right)^{1/3} \quad 4.21$$

Where

$$dr_{in} = \frac{D_{r,\text{int}}}{\Delta z} \quad 4.22$$

For turbulent flow case where  $(3000 < \text{Re} < 5 \times 10^6)$  and  $(0.5 \leq \text{Pr} \leq 2000)$  Gnieliski correlation can be used (equation (4.23)) [34]:

$$Nu_{tur} = \frac{\left(\frac{f}{8}\right)(\text{Re}-1000)\text{Pr}}{1+12.7\sqrt{\frac{f}{8}}(\text{Pr}^{2/3}-1)} \quad 4.23$$

Where  $f$  is the friction factor for same range of Reynold number and defined by:

$$f = (0.79 \ln \text{Re} - 1.64)^{-2} \quad 4.24$$

In the transient region where  $(2300 \leq \text{Re} \leq 3000)$  Gnielinski proposed equation (4.25):

$$Nu_f = (1-\zeta)Nu_{lam} + \zeta Nu_{tur} \quad 4.25$$

Where

$$\zeta = \frac{\text{Re}_f - 2300}{3000 - 2300} \quad 4.26$$

Heat transfer coefficient for fluid inside the receiver tube from equation (4.27) calculated:

$$h_{f,j} = \frac{k_j Nu_j}{D_{r,in}} \quad 4.27$$

Mean heat transfer coefficient at center of control volume

$$\bar{h}_{f,j} = \frac{h_{f,j+1} + h_{f,j}}{2} \quad 4.28$$

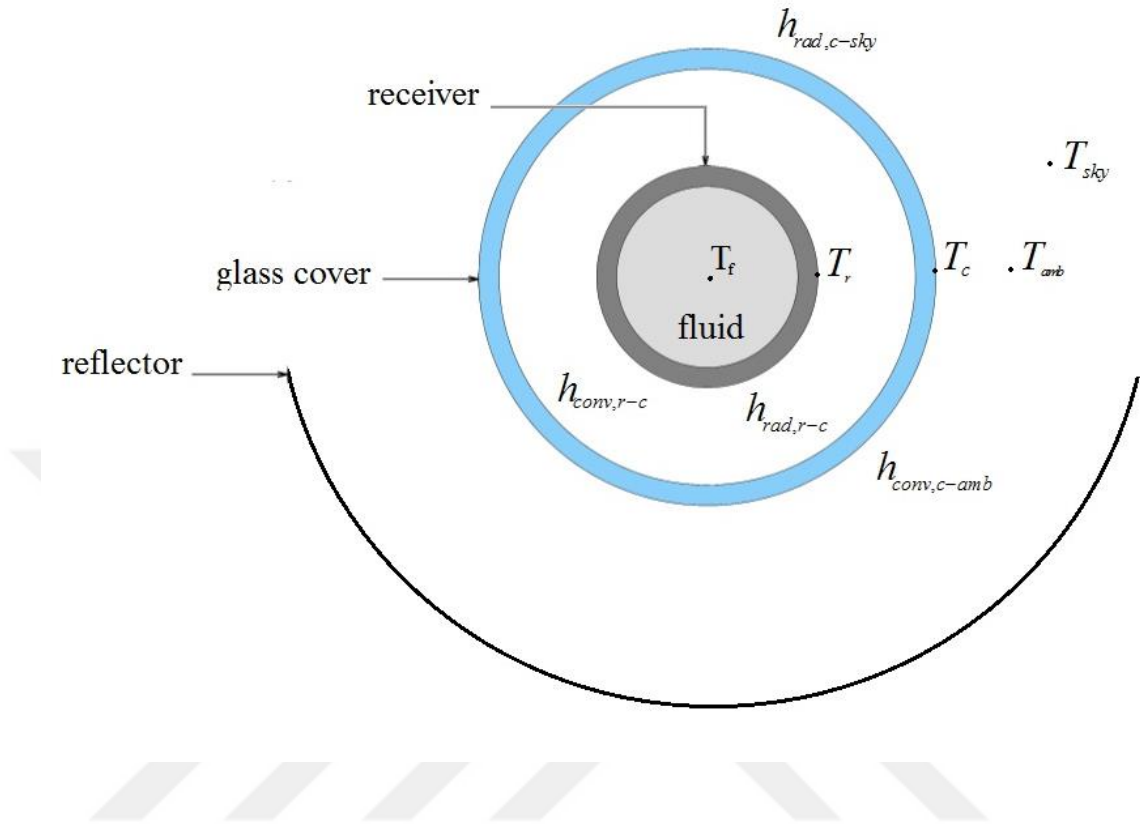


**Figure 4.2:** Heat transfer numen-culture for solar (PTC)

### 4.3 Receiver tube wall analysis

Finite volume method (FVM) have been used in the simulation of receiver tube wall. The variation of temperature in axial direction has been detected. After integrating conduction equation over a control volume for receiver tube wall the following equation obtained for each CV[10]:

$$a_j T_{r,j} = b_j T_{r,j+1} + c_j T_{r,j-1} + d_j \quad 4.29$$

Where the coefficients:

$$a_j = b_j + c_j + \bar{h}_{f,j} \pi D_{r,int} \Delta z + \frac{A_{t,r} \Delta z}{\Delta t} \rho c_p \quad 4.30$$

$$b_j = \frac{k_r A_{t,r}}{\Delta z} \quad 4.31$$

$$c_j = \frac{k_r A_{t,r}}{\Delta z} \quad 4.32$$

$$d_j = \left( \bar{h}_{f,j} \pi D_{r,int} \bar{T}_{f,j} + \dot{q}_{u,j} \pi D_{r,ext} \right) \Delta z + \frac{A_{t,r} \Delta z}{\Delta t} \rho c_p T_{r,j}^o \quad 4.33$$

The coefficients can apply for  $(2 \leq j \leq n_z - 1)$  (Figure 4.3). The axial heat conduction and temperature boundary conditions are taken into account for coefficients estimation. Every term which contains time will be neglected since a steady state assumed so (a and d) coefficients become:

$$a_j = b_j + c_j + \bar{h}_{f,j} \pi D_{r,int} \Delta z \quad 4.34$$

$$d_j = \left( \bar{h}_{f,j} \pi D_{r,int} \bar{T}_{f,j} + \dot{q}_{u,j} \pi D_{r,ext} \right) \Delta z \quad 4.35$$

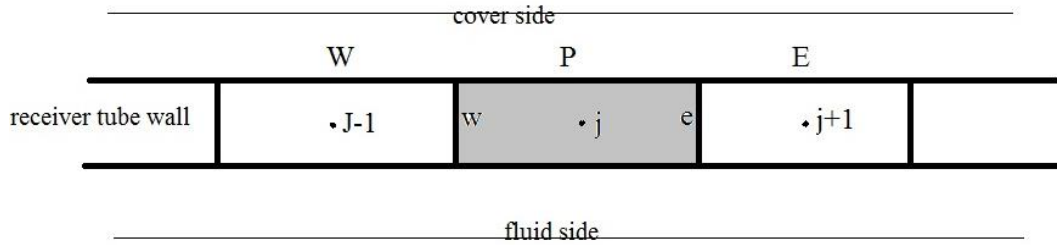


**Figure 4.3:** Characteristics control volume receiver wall

For first and last CV ( $j = 1$  and  $j = n$ ) boundary condition which applied for first control volume temperature is assumed and for last control heat flux equals zero since isolation end assumed for receiver wall as explained in Figure 4.4'. The application of boundary condition involved (a and d) coefficients and it results:

$$a_1 = c_1 + \bar{h}_{f,1} \pi D_{r,int} \Delta z + \frac{2}{\Delta z} \quad 4.36$$

$$d_1 = \left( \bar{h}_{f,1} \pi D_{r,int} \bar{T}_{f,1} + \dot{q}_{u,1} \pi D_{r,ext} \right) \Delta z + 2 \frac{T_B}{\Delta z} \quad 4.37$$

$$a_n = b_n + \bar{h}_{f,n} \pi D_{r,int} \Delta z \quad 4.38$$

$$d_n = \left( \bar{h}_{f,n} \pi D_{r,int} \bar{T}_{f,n} + \dot{q}_{u,n} \pi D_{r,ext} \right) \Delta z \quad 4.39$$

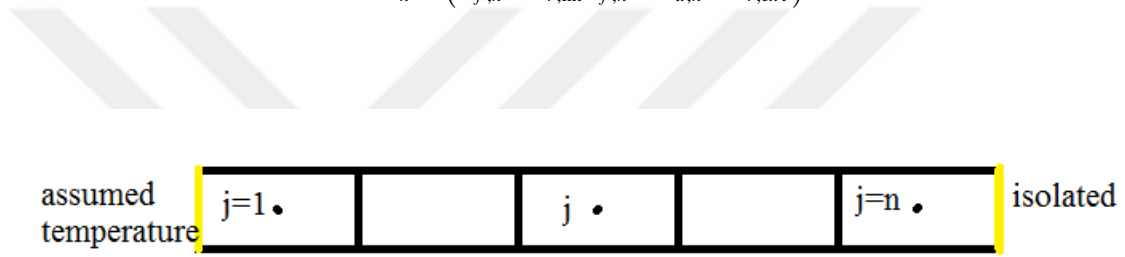


**Figure 4.4:** Characteristics control volume receiver wall and glass cover wall for first and last control volume

#### 4.4 Glass cover temperature

The same procedure for receiver has applied for glass cover with air in the space gap and steady state condition. Equation (4.40) have discretized which is applicable for entire control volumes.

$$a_j T_{c,j} = b_j T_{c,j+1} + c_j T_{c,j-1} + d_j \quad 4.40$$

Where the coefficients applied for all control volume except first and last CV:

$$a_j = b_j + c_j + \left( h_{conv,c\_amb,j} + h_{rad,c\_sky,j} \right) \pi D_{c,ext} \Delta z + \left( h_{rad,r-c,j} + h_{conv,r-c,j} \right) \pi D_{c,in} \Delta z \quad 4.41$$

$$b_j = \frac{k_c A_{t,c}}{\Delta z} \quad 4.42$$

$$c_j = \frac{k_c A_{t,c}}{\Delta z} \quad 4.43$$

$$d_j = \left( (h_{conv,c-amb,j} + h_{rad,c-sky,j}) \pi D_{c,ext} T_{amb} + (h_{rad,r-c,j} + h_{conv,r-c,j}) \pi D_{c,in} T_{r,j} \right) \Delta z + \dot{q}_{loss,j} \pi D_{c,ext} \Delta z \quad 4.44$$

After applying boundary conditions for first and last control volume by the same way that applied for receiver wall as shown in Figure 4.4' the (a and d) coefficient re-introduced to:

$$a_1 = c_1 + (h_{conv,c-amb,1} + h_{rad,c-sky,1}) \pi D_{c,ext} \Delta z + (h_{rad,r-c,1} + h_{conv,r-c,1}) \pi D_{c,in} \Delta z + \frac{2}{\Delta z} \quad 4.45$$

$$d_1 = \left( (h_{conv,c-amb,1} + h_{rad,c-sky,1}) \pi D_{c,ext} T_{amb} + (h_{rad,r-c,1} + h_{conv,r-c,1}) \pi D_{c,in} T_{r,1} \right) \Delta z + \dot{q}_{loss,1} \pi D_{c,ext} \Delta z + 2 \frac{T_B}{\Delta z} \quad 4.46$$

$$a_n = b_n + (h_{conv,c-amb,n} + h_{rad,c-sky,n}) \pi D_{c,ext} \Delta z + (h_{rad,r-c,n} + h_{conv,r-c,n}) \pi D_{c,in} \Delta z \quad 4.47$$

$$d_n = \left( (h_{conv,c-amb,n} + h_{rad,c-sky,n}) \pi D_{c,ext} T_{amb} + (h_{rad,r-c,n} + h_{conv,r-c,n}) \pi D_{c,in} T_{r,n} \right) \Delta z + \dot{q}_{loss,n} \pi D_{c,ext} \Delta z \quad 4.48$$

Evacuated tubular covered case is same as non-evacuated tubular cover the only different in the evacuated situation is convective heat transfer coefficient in the annulus ( $h_{conv,r-c}$ ) assumed to be zero. And in the no cover case the terms which related to glass neglected, Only two heat transfer coefficients exists they are ( $h_{conv,r-amb}$ ) and ( $h_{rad,r-sky}$ ) and they have introduced by equations (4.4) and (4.5) respectively.

#### 4.5 Optical and thermal efficiency:

The optical efficiency for solar PTC is defined in the following form [10, 33]:

$$\eta_{op} = \frac{S_r}{I_b} \quad 4.49$$

The solar (PTC) thermal efficiency is defined by the following formula [6, 10, 27, 33]:

$$\eta_{th} = \frac{\dot{Q}_u}{A_{ref} I_b} \quad 4.50$$

Where ( $\dot{Q}_u$ ) is the amount of heat absorbed by fluid flowing in the receiver tube [6, 9, 27, 29, 36].

$$\dot{Q}_u = \dot{m}Cp(T_{f,out} - T_{f,in}) \quad 4.51$$

#### 4.6 Solution time for the code:

In the current study Matlab program has been used in order to get the result. Two different code have written:

First: equation for properties have defined in separated code for each powder ratio. Then they run together in one code for plotting the result and showing the effect of powder ratio addition on the base fluid. This running is take three minutes.

Second: entire equations for other steps defined in the code and merged with previous part in order to become one code. As the inputs applied in the code the work is verified with acceptable result. This step takes one tow minute.

Third: after verification three parameters have been changed (solar radiation, fluid inlet temperature and volume flow rate). The code has run in 13 minutes for each parameter.

Fourth: for evacuated cover case four deferent fluid inlet temperature assumed and the effect of powder ratio as a function of volume flow rate have defined. This code has run in 95 minutes.

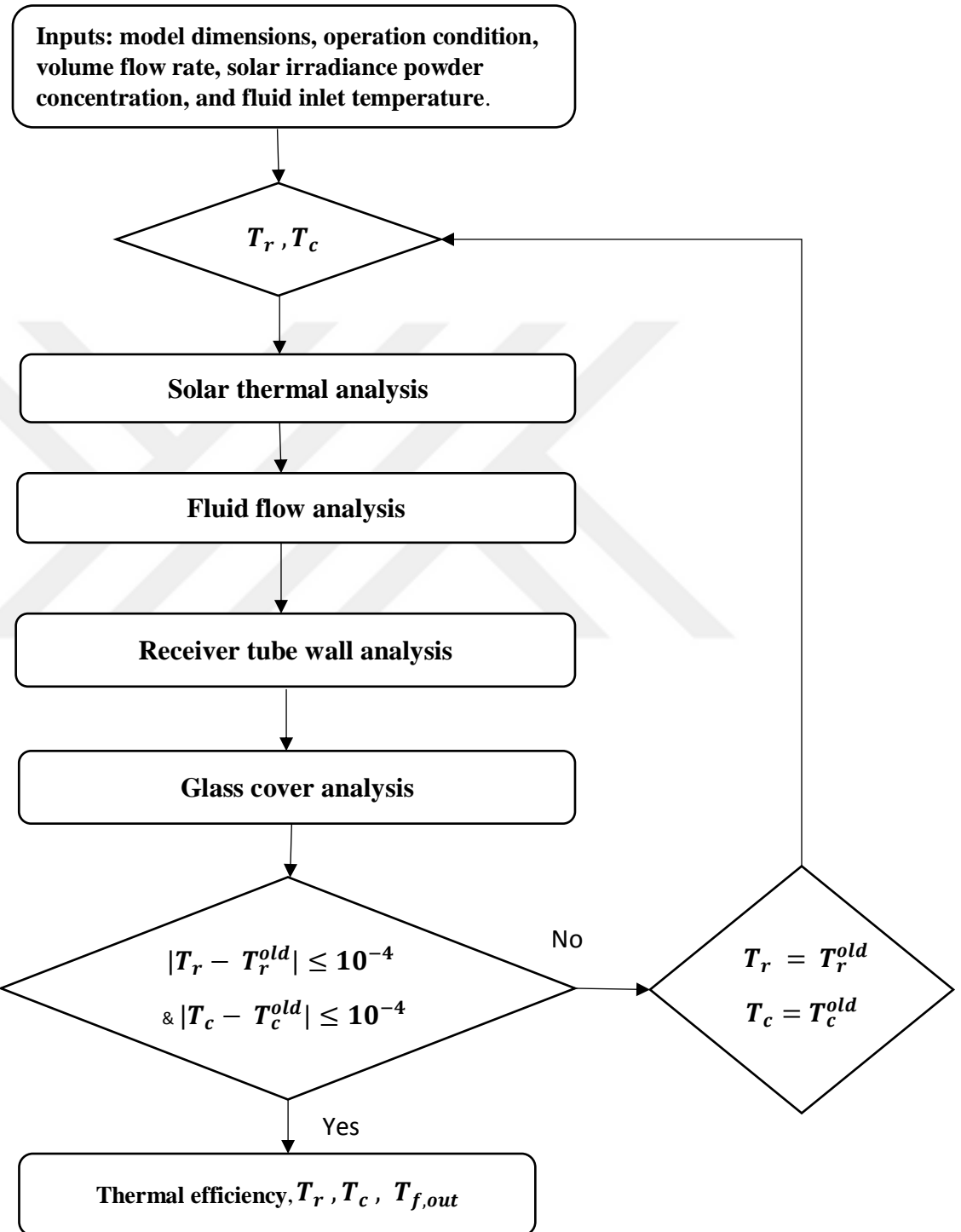


Figure 4.5 : Simulations block diagram



## CHAPTER FIVE

### RESULT AND DISCUSSION

#### 5.1 Fluid Properties

Simulation result for SPTC strongly depends on the circulated fluids property. The property for the used fluid is given by polynomial which is temperature dependent. The polynomials applicable for a wide range of temperature (absolute in Kelvin) ( $273.15 \leq T \leq 673$ ). Fluids properties also changing when nanoparticles of aluminum oxide is adding to it for improving thermal properties. The addition of nanoparticles always is in limited range between (1% and 8%). Exceeding the mentioned limit may cause some problems such as corrosion[9]. It is only the base fluid when nanoparticles' concentration is zero.  $\text{Al}_2\text{O}_3$  powder was added as Nano-particles. The following sections obtaining explanation for each property at different temperature and concentration of aluminum powder.

##### 5.1.1 Specific heat capacity

Figure 5.1' shows the relationship of specific heat with temperature and Nano-particles in different percentage. As ( $\phi = 0\%$ ) which its curve appears in black. It defines the specific heat of Synthetic oil which is the highest one in the absence of powder. And increasing of powder concentration is resulting less change in specific heat with temperature. For instant blue curve contains lower specific heat than red, green and black also less change with temperature comparing with mentioned before. Figure 5.2' expressing the effect of powder addition to synthetic oil at (300 K, 450 K, 600 K) in three curves. It denoted that Specific heat is decreasing by increasing aluminum powder in the base fluid. But declining in the highest temperature is the most one among the others as it shown in blue curve in Figure 5.2'.

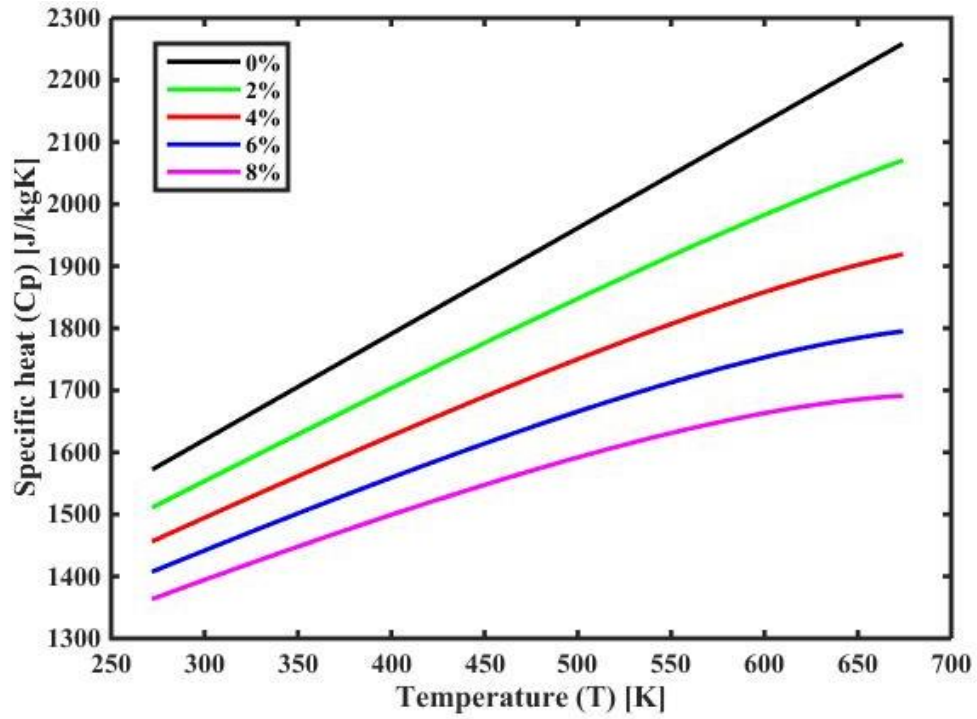


**Figure 5.1:** Specific heat capacity as a function of temperature and different powder concentration

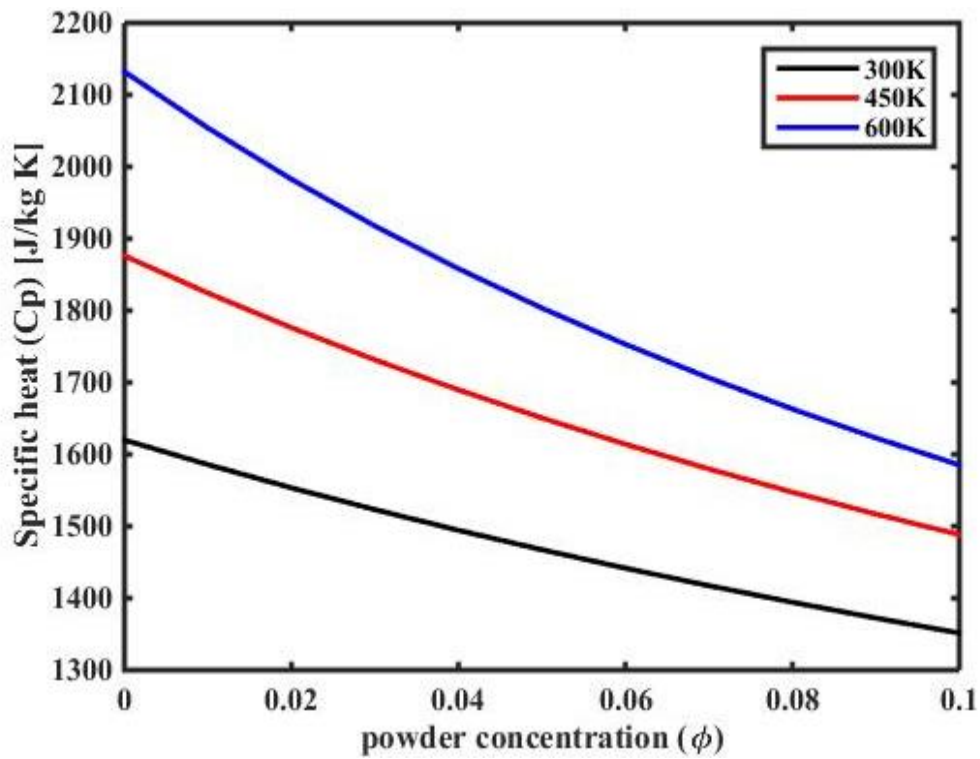


**Figure 5.2:** Specific heat as a function of powder concentration and temperature.

### 5.1.2 Thermal conductivity

In Figure 5.3' black curve is the thermal conductivity of synathitic oil which has the lowest value. The thermal conductivity of the fluid is decreasing proportionally with temperature raising. The effect of powder concentration is appearing in (green, red, blue and magenta) curves and how it is rising thermal conductivity. Thermal conductivity lines slope growing with temperature by rising the value of Nano-fluid . Such as a magenta line ( $\varphi = 8\%$  ) has a greater slope than a green line ( $\varphi = 2\%$  ) that lead to heat transfer enhancement. Figure 5.4' showing the direct impact of powder concentration at three different temperature. This effect is larger at low temperature and it became less at a higher temperature. For example, blue curve in Figure 5.4' which at (600 K) is less raised with powder concentration in a comparing with black curve.

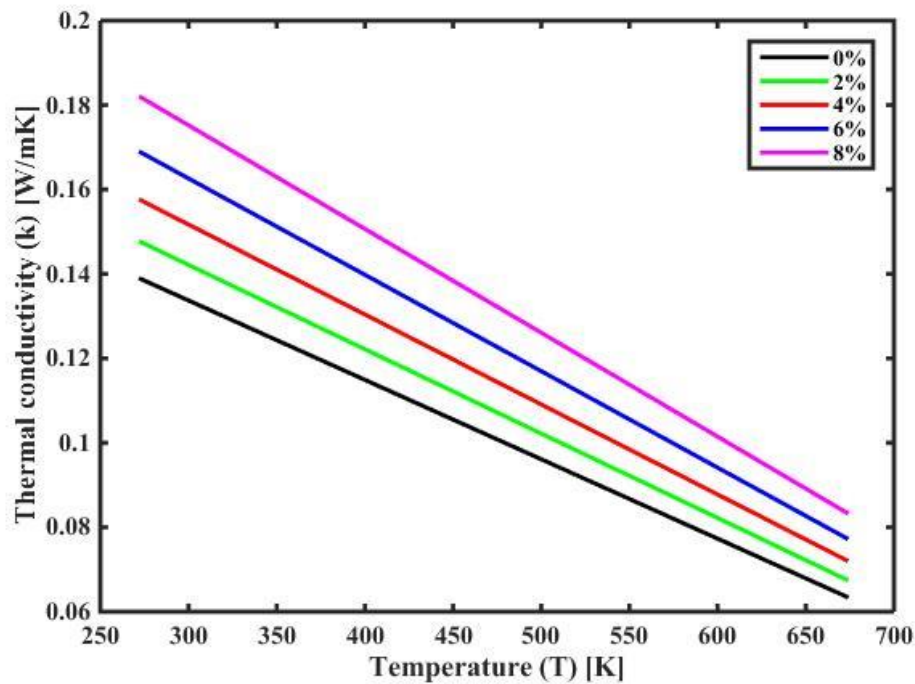


**Figure 5.3:** Thermal conductivity as a function of temperature and powder concentration.

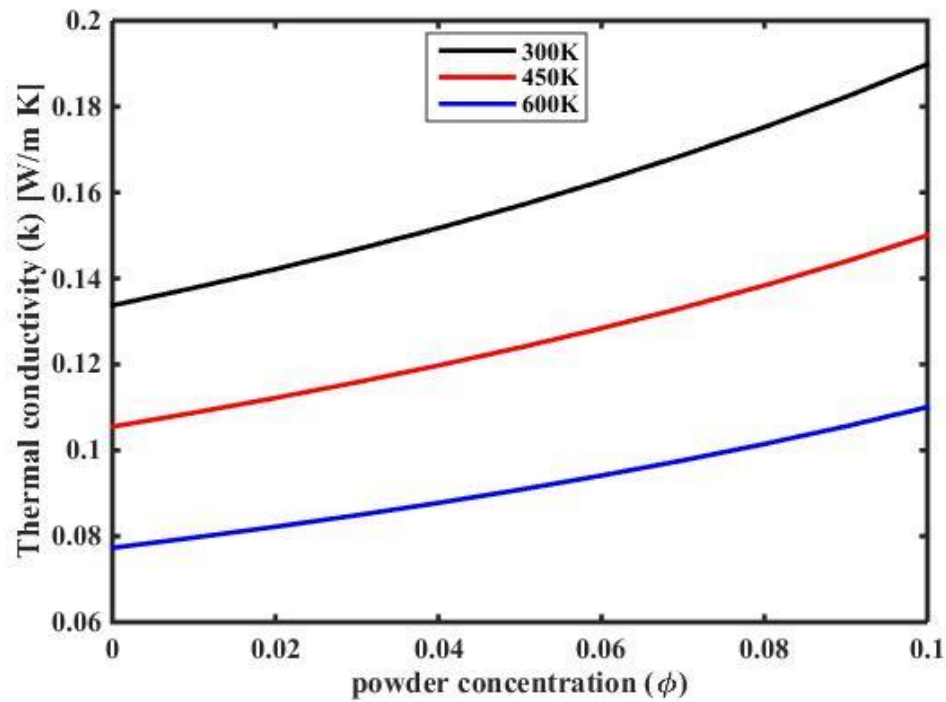


**Figure 5.4:** Influencing of thermal conductivity by powder concentration at (300 K, 450 K and 600 K).

### 5.1.3 Density

Density manipulating with temperature and powders ratio in the base fluid as is detected by Figure 5.5'. It shows that synthetic oil and Nano-fluids density decreasing with temperature increasing. Figure 5.6' explains the influencing of density by nanoparticles ratio in the base fluid at (300 K, 450 K, 600 K). Its density became more and more by ascending the nanoparticles ratio in the fluid. But the increasing is not different for high or low temperature.

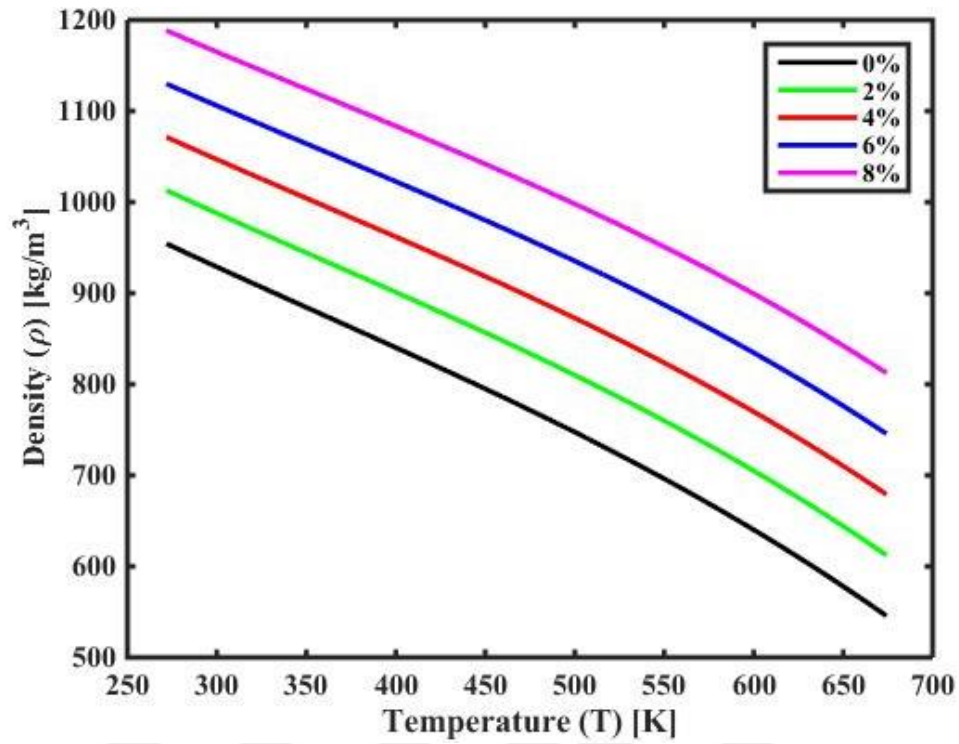


**Figure 5.5:** Density as a function of temperature and different powder concentration.

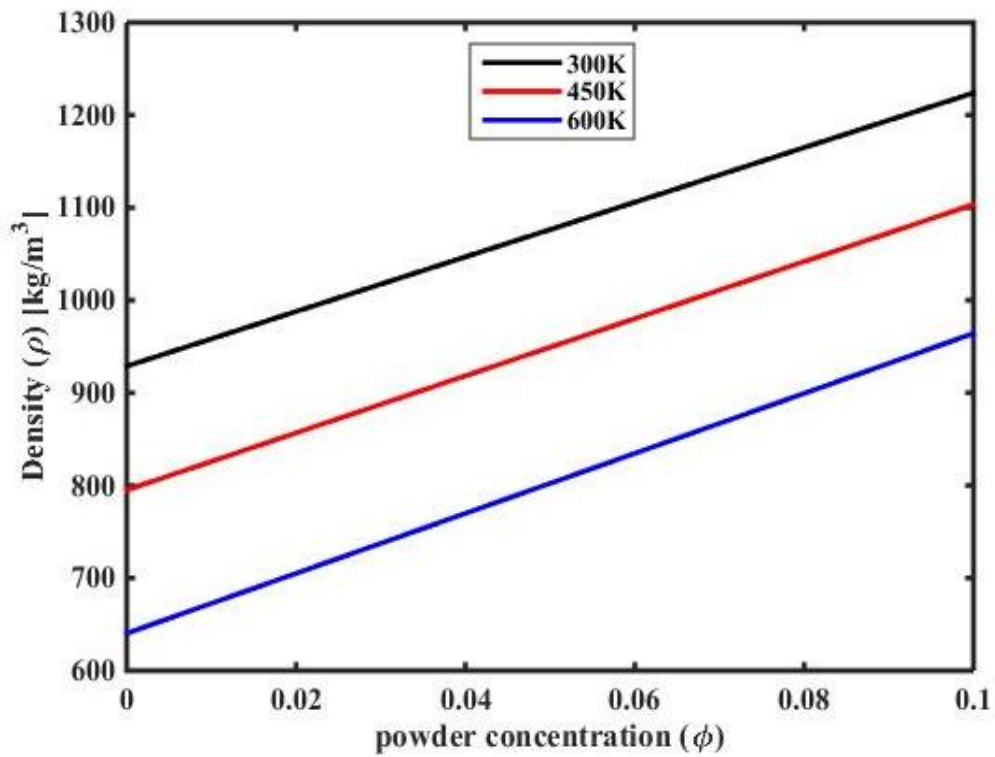


**Figure 5.6:** Influencing of density by powder concentration at (300K, 450K and 600K).

#### 5.1.4 Dynamic viscosity

Figure 5.7' shows the impact of temperature and the ratio of nano-particles on the dynamic viscosity. It is manipulating adversely with increasing in temperature and it shaped in a parabolic curve with a pulse in it (between temperature 340K to 350K) due to the high order variable ( $T^6$ ) in its polynomial. Figure 5.8' viewing that at low temperature adding more amount of powder effectively increasing dynamic viscosity as the black curve at (300K) explaining that. As the temperature is rising the effect of the nano-particles ratio is become less and less, For example, blue curve is denoting (600 K) in Figure 5.8' the dynamic viscosity affected less by powder concentration than the other curves in the same figure.

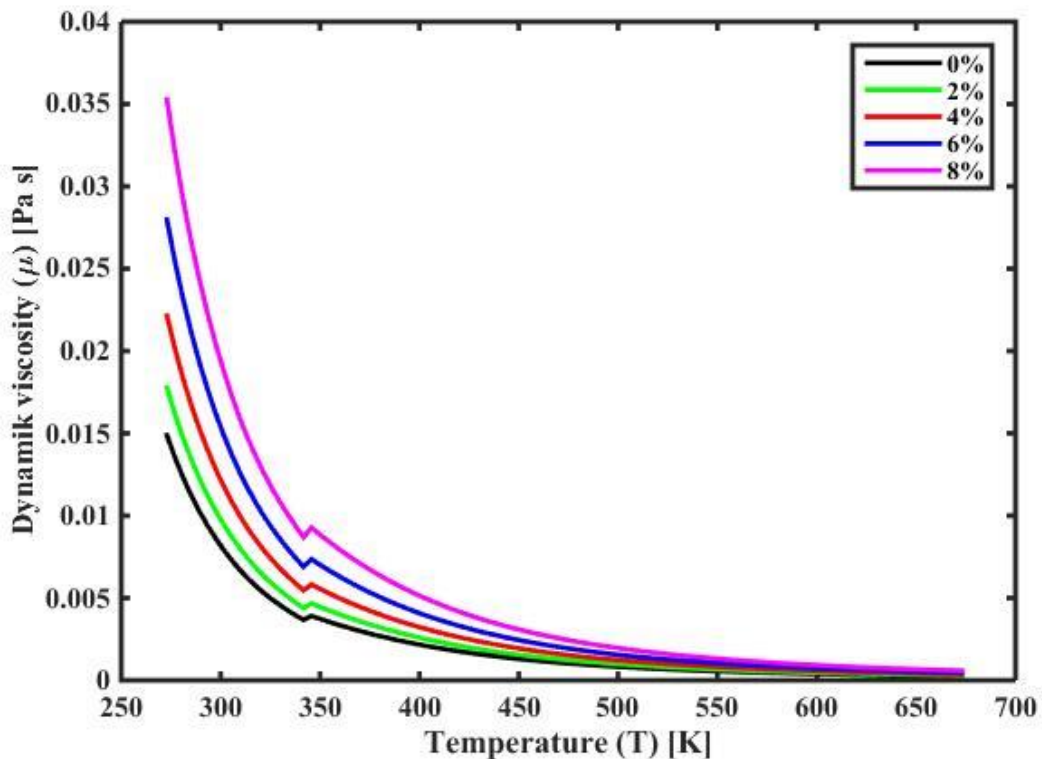


**Figure 5.7:** Dynamic viscosity as a function of temperature and different powder concentration

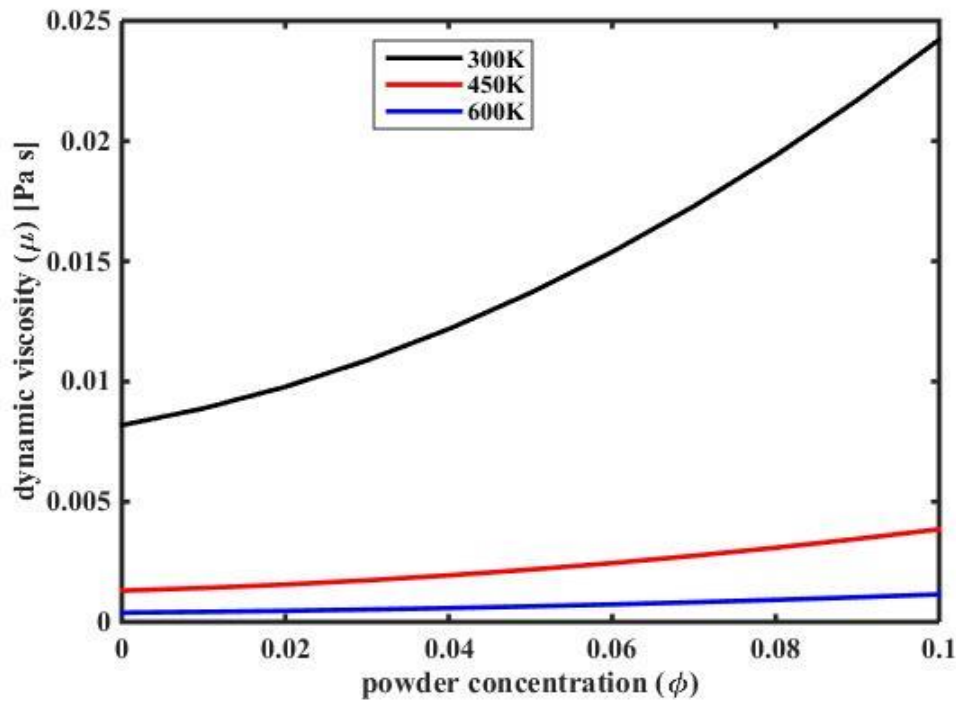


**Figure 5.8:** Influencing of dynamic viscosity by powder concentration at (300 K, 450 K and 600 K)

### 5.1.5 Prandtl number

Figure 5.9' detects how Prandtl number is decreasing with inflating in temperature for different powders concentration. Prandtl number is a function of dynamic viscosity, specific heat and thermal conductivity. It shaped in a parabolic curve with a jump in it. Its curve influenced dynamic viscosities curves because of rapidly changing in the value of dynamic viscosity in low temperature and dynamic viscosities in the nominator in the Prandtl numbers equation. In addition of high order variable ( $T^6$ ) in dynamic viscosities polynomial. Also, the value of Prandtl number increased because of the high value of specific heat. Figure 5.10 expressing the addition in the amount of nano-particles on Prandtl number. Powders concentration effect is greater at low temperature than in high temperature. As it shows in Figure 5.10 black curve (at 300 K) is more affecting by powders ratio than the red curve (at 450 K) and the red one is more affected than the blue one (at 600 K).

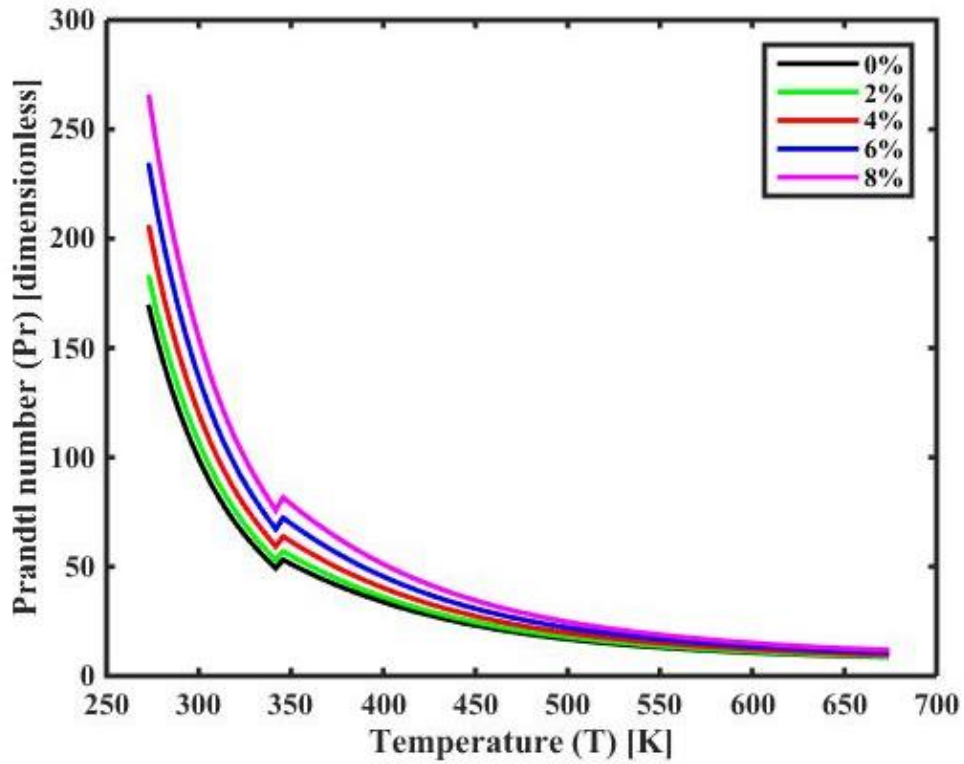


**Figure 5.9:** Prandtl number as a function of temperature and different powder concentration

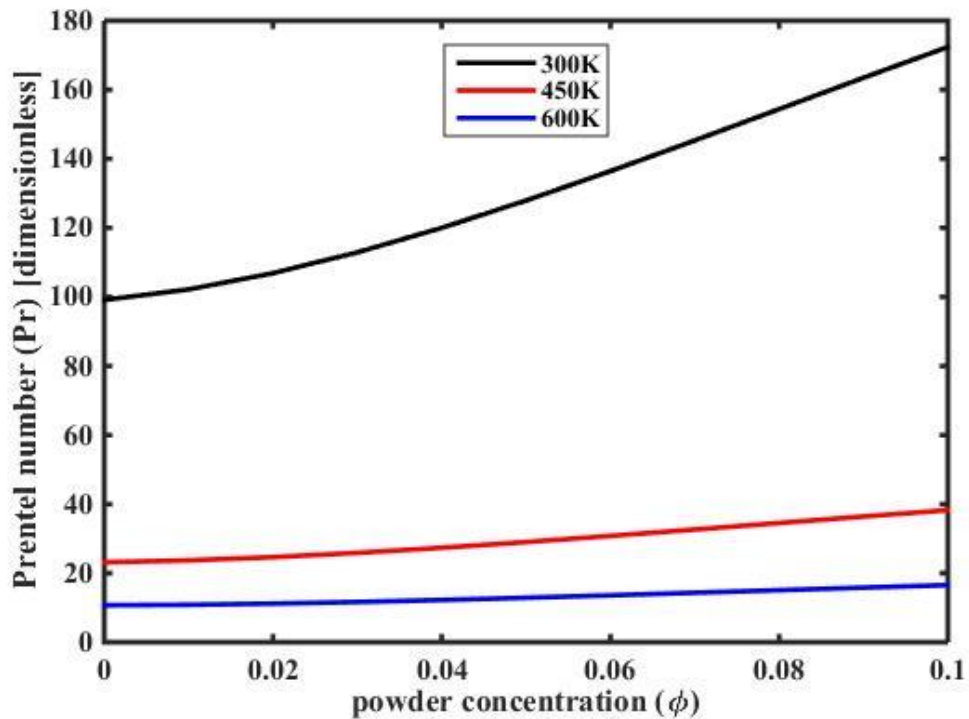


**Figure 5.10:** Influencing of Prandtl number by powder concentration at (300 K, 450 K and 600 K)



## 5.2 Verification processes steps

In order to verify current work the model and experimental results from Sandia National Laboratory have taken (as shown in Table 3') and comparing with current work

**Table 2:** PTC specifications and design dimensions used in the model validation (SNLM) from [10]

Receiver length	7.8 m
Collector width	5 m
Focal distance	1.84 m
Receiver internal diameter	0.066 m
Receiver external diameter	0.070 m
Glass cover internal diameter	0.115 m
Glass cover external diameter	0.109 m
Receiver tube thermal conductivity	54 W/m K
Concentration ratio	22.42
Receiver absorptance	0.906
Receiver emittance	0.14
Glass cover transmittance	0.95
Reflected surface reflectivity	0.93
Shape factor	0.92
Inclination angle	0.0
Incident angle modifier	1.0
Optical efficiency	0.736

**Table 3:** Experimental data from Sandia National Laboratory compared with numerical analysis.

	Input					Result	
	$I_b$ (W/m <sup>2</sup> )	Flow rate (l/min)	Wind speed (m/s)	$T_{amb}$ (°C)	$T_{inlet}$ (°C)	$\Delta T_{exp}$ (°C)	$\eta_{th}$ (%)
experimental	906.7	55.4	0	31.7	299.5	17	62.39
numerical	906.7	55.4	0	31.7	299.5	16.86	62.09

### 5.2.1 Temperatures distribution along the collector

Temperatures distribution along the collector have been calculated and plotted in the Figure 5.11'. Receiver tube, fluid and glass cover temperatures have explained by blue, green and red colors respectively. The effect of boundary conditions appears at the beginning of receiver and cover. the receiver tube has the highest temperature because of high absorptivity of the receiver tube and low emissivity for solar irradiance vice versa for glass cover which has the lowest temperature. The fluid temperature should be between them as appears by green line. Receiver and cover influencing fluid temperature rising along the receiver.

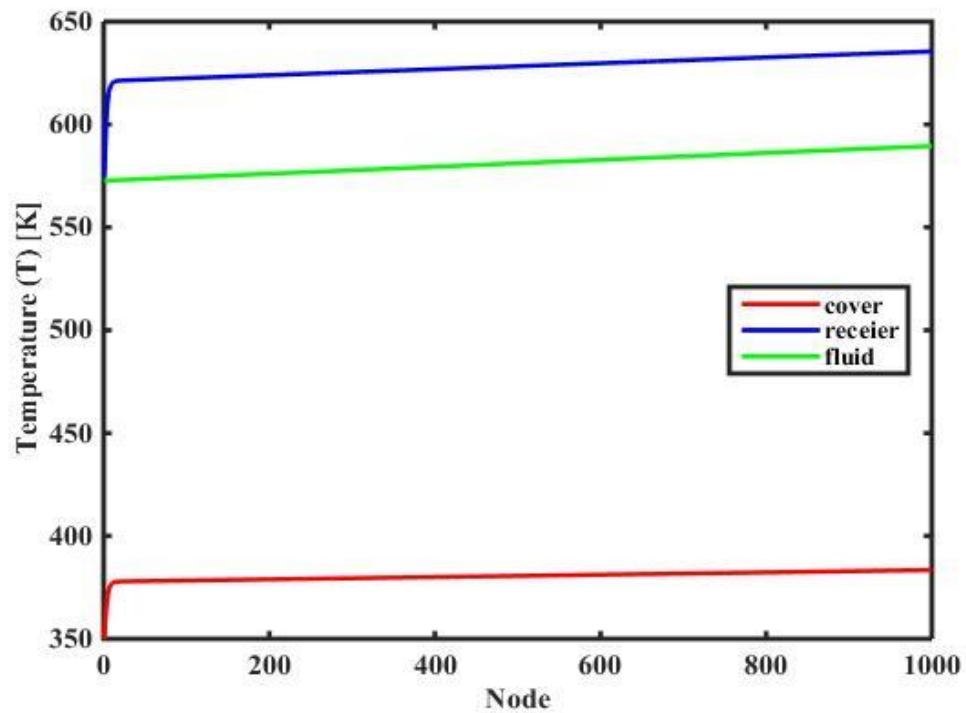


**Figure 5.11:** Temperatures profile along the collector

### 5.2.2 Reynold number along the collector

Reynold number is strongly dependent on flow rate and on the fluid properties. Volume flow rate (55.4 L/min) have been used at inlet section which gives a high Reynold number ( $2.55 \times 10^4$ ) in the turbulent region and fluid properties are very sensitive to temperature as shown in Figure 5.1' to Figure 5.8'. The changes in properties with temperature leading to increasing in Reynold number along with the receiver tube as Figure 5.12' is explaining it.

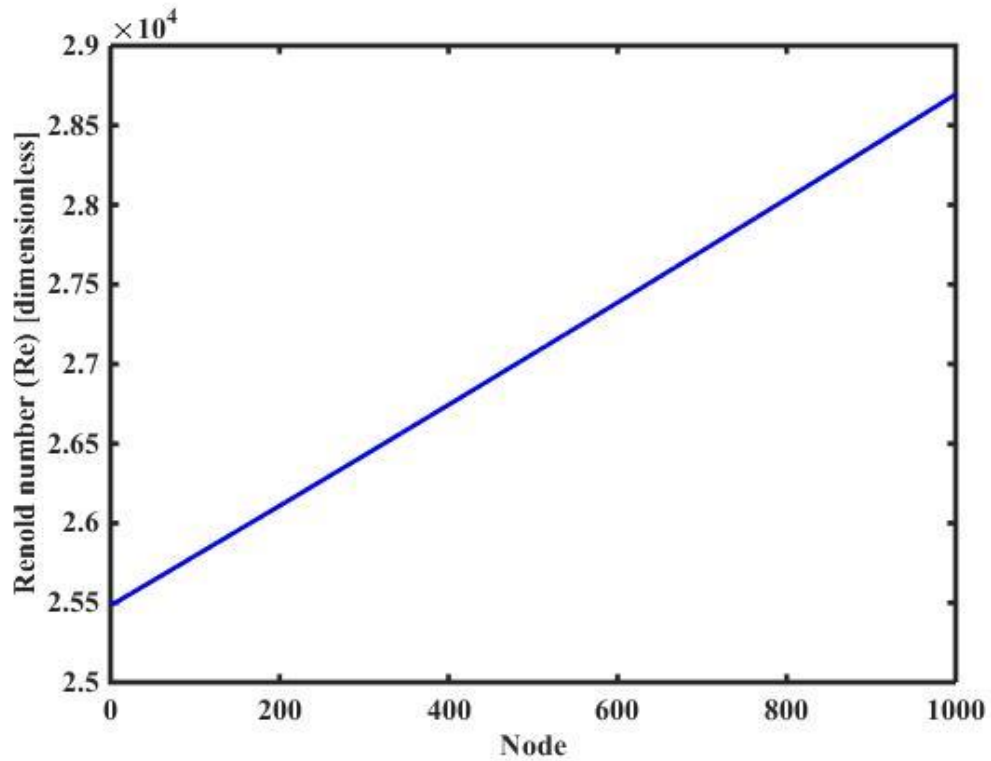


**Figure 5.12:** Reynold number changing inside receiver tube along the collector

### 5.2.3 Nusselt number along the collector

Nusselt number enhancement has investigated by Reynold number rising despite declining in Prandtl number since change in Reynold number is much more than the change in Prandtl number. In the Figure 5.13' it is indicated that how Nusselt numbers value enlarged from (226-244). More Explanations have been plotted in Figure 5.14' in order to show the influencing of the Nusselt number by Reynold number along with the tube.

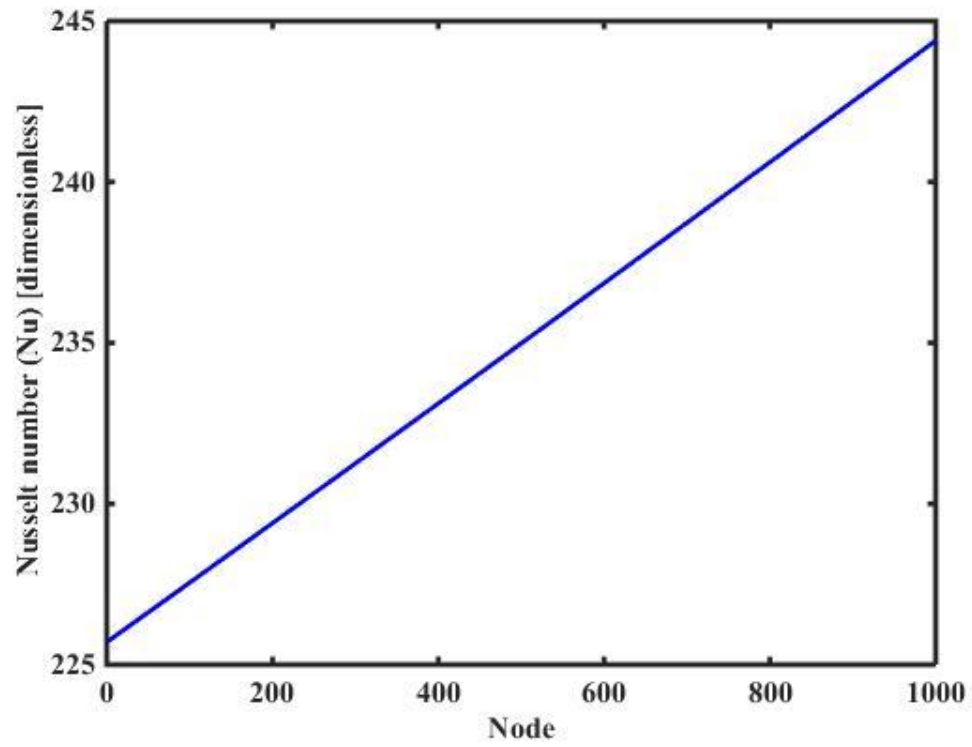


**Figure 5.13:** Nusselt number along the collector

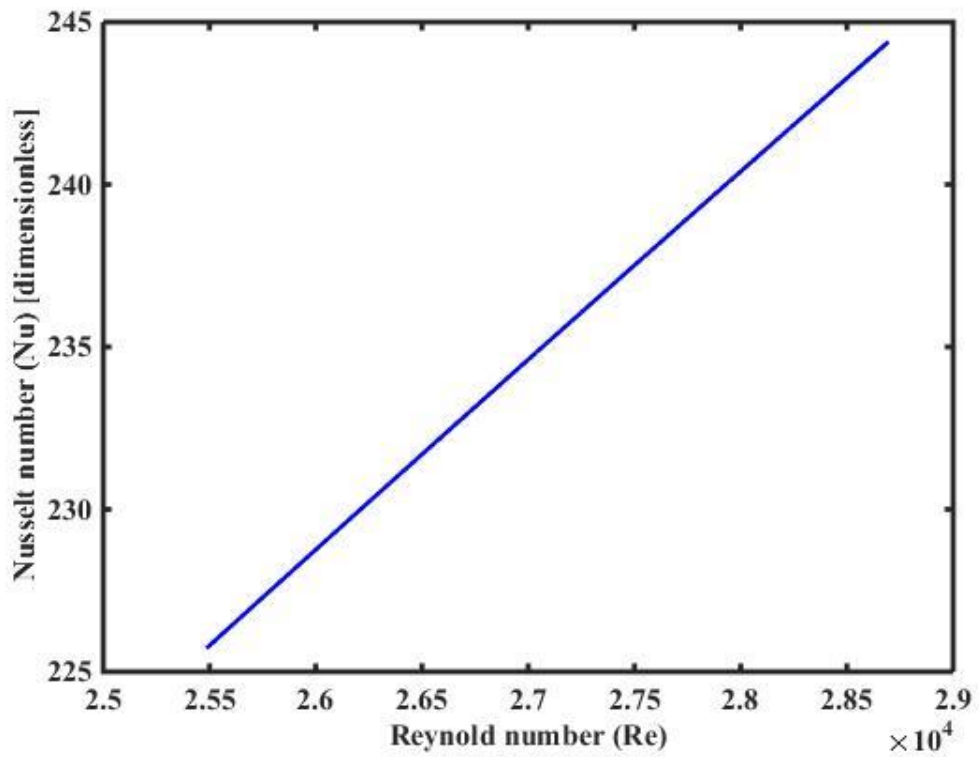


**Figure 5.14:** Relation between Reynolds number and Nusselt number

### 5.2.4 Heat transfer coefficient

In order to get more accurate result, heat transfer coefficient should be evaluated locally. It is a must of collector's simulation to know what is happening inside in receiver tube. As expressed in Figure 5.15' heat transfer coefficient is arises among the length of receiver which is a great influencing of Nusselt number.

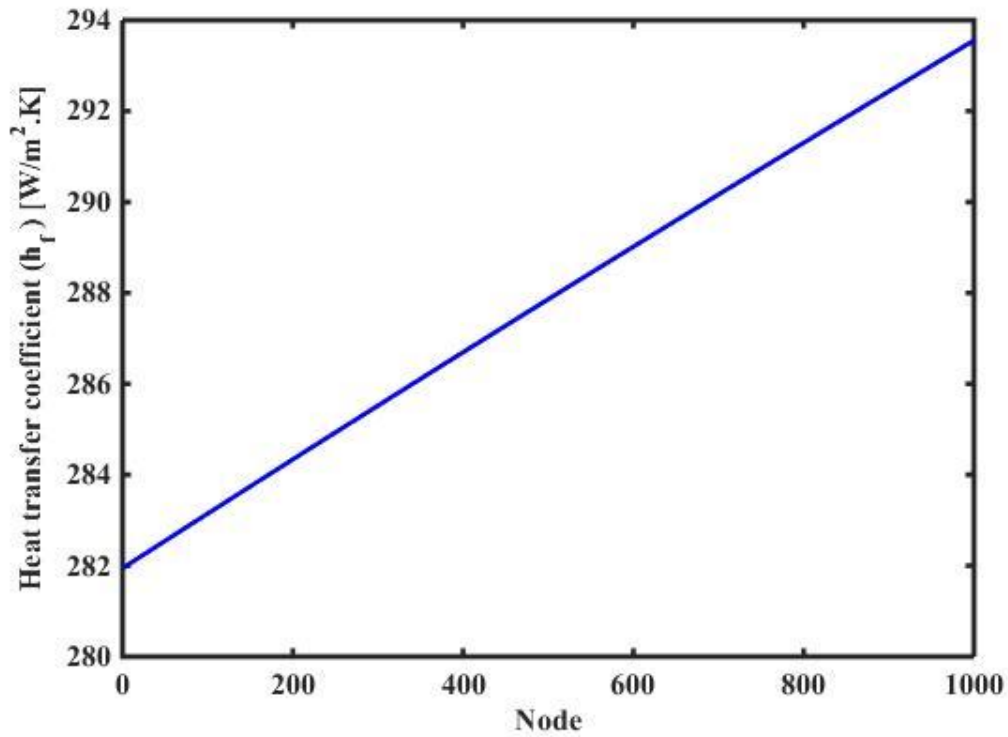


**Figure 5.15:** Heat transfer coefficient inside the receiver tube.

### 5.2.5 Heat flux along the collector

Heat flux into two different directions have been considered. Heat gain is that amount of energy which absorbed by the fluid via the metallic receiver tube wall. The effect of boundary condition clearly presented in the Figure 5.16' for both heat gain and heat loss. There is slightly decreasing in heat gain along the receiver vice versa for heat loss which caused by convection and radiation from the outer surface of glass cover with ambient.

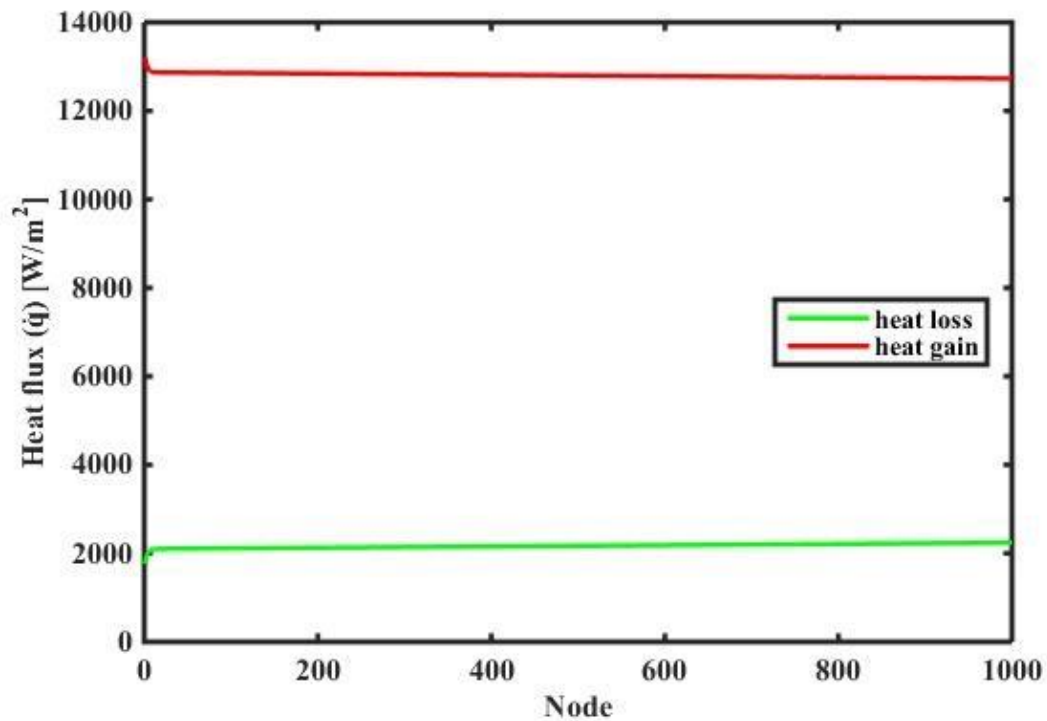


**Figure 5.16:** Heat flux along the receiver.

### 5.2.6 Effect of temperature on heat flux distribution

Temperature is a very strong parameter of heat flux, as shown in Figure 5.17' when receiver temperature increase along the collector (black curve) because of increasing in fluid temperature (red curve), the useful heat flux which is defined by magenta collar curve is decrease due to radiation and convection from outer side of the receiver. Whereas the receiver temperature is increasing the heat loss is influencing it which is shown by green curve.

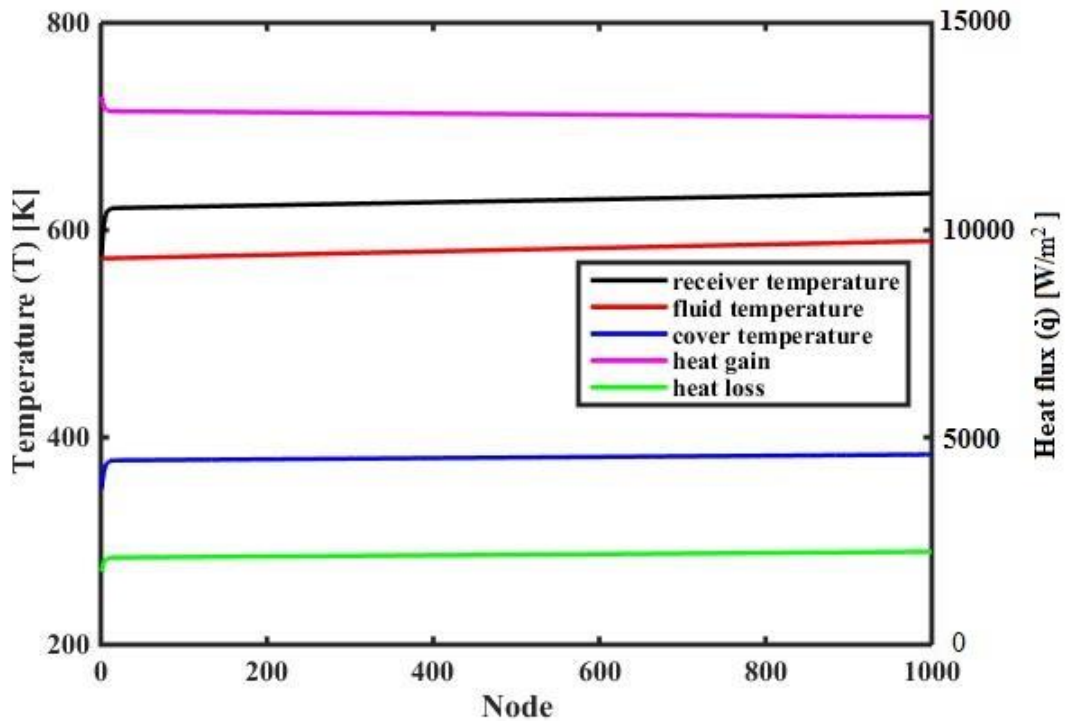


**Figure 5.17:** Temperature and heat flux distribution along the collector.

After these steps, the result has appeared in the new analysis by using different HTF. The gotten thermal efficiency has a good agreement with the experimental one where equaled (62.09 %). It is different from experimental model work by (0.3 %). This difference is caused by using different heat transfer fluid.

### 5.3 Different fluid inlet temperature

#### 5.3.1 Effect of fluid inlet temperature on the outlet temperature.

After verification steps, the simulation has carried out on the same condition of verification case. But a different range of inlet fluid temperature (400-650K) has applied, the temperature between inlet and outlet has plotted by three different colors for without cover receiver, evacuated cover and non-evacuated cover receiver in the Figure 5.18'. It indicates that at low inlet temperature there is on big different between the outlet temperature for all cases but by rising fluid inlet temperature the different between outlet temperatures slightly appears. The outlet temperature for evacuated case has the highest



value since it has the best thermal isolation with its environment vice versa for coverless. And non-evacuated case is between them. Figure 5.19' shows the enlarged section for Figure 5.18' at low inlet temperature (448K to 456K) and high inlet temperature (596K to 606K).

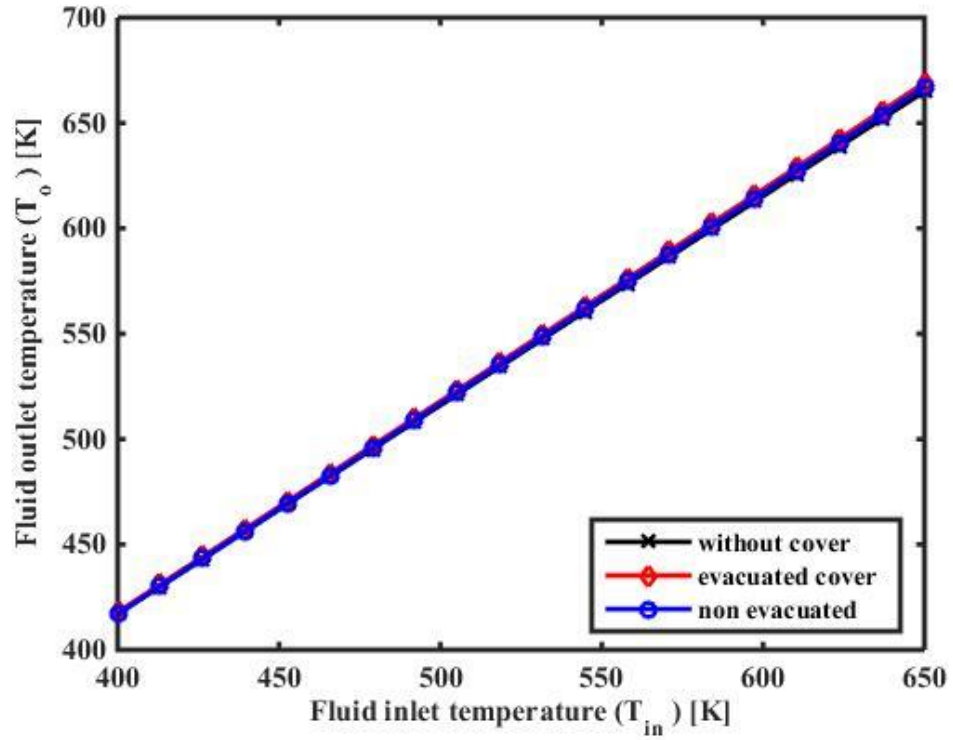


**Figure 5.18:** Relationship between inlet and outlet fluid temperature.

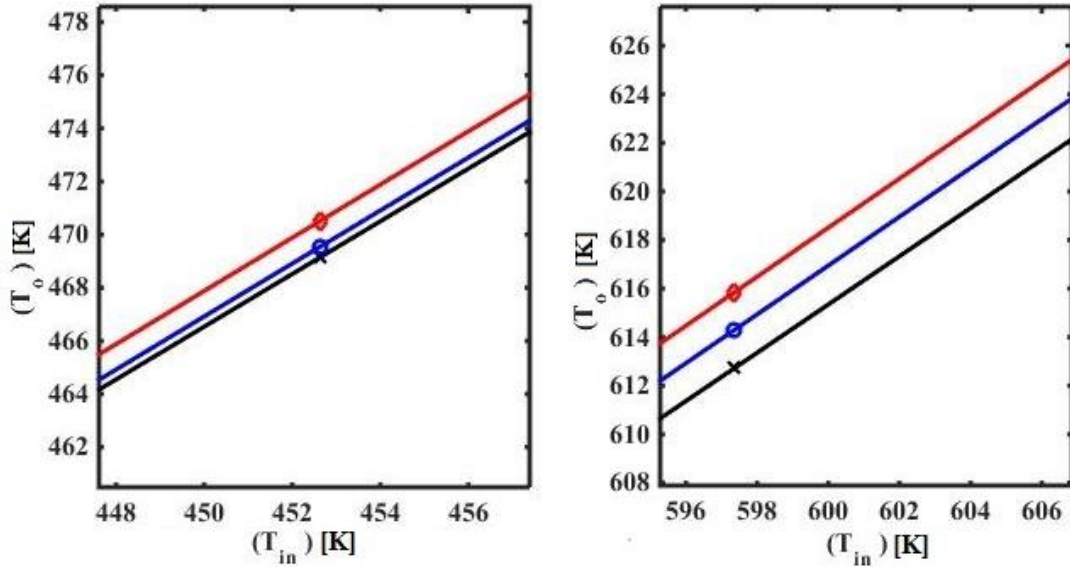


**Figure 5.19:** Enlarged section relationship between inlet and outlet fluid temperature.

### 5.3.2 Effect of fluid inlet temperature on the heat gain

When heat gain has the greatest value heat loss has the smallest magnitude for all cases. At the low temperature, all cases heat gain has a higher value than at higher temperature due to the small magnitude of a temperature different between ambient and glass cover as explained in Figure 5.20'. But as temperature became higher and higher by the effect of isolation occurred by the cover and evacuation which is resulting the best heat gain for evacuated case and denoting by the red curve. After that non-evacuated case which has a value between other cases. Finally, without cover has the lowest value of energy gain by black curve.

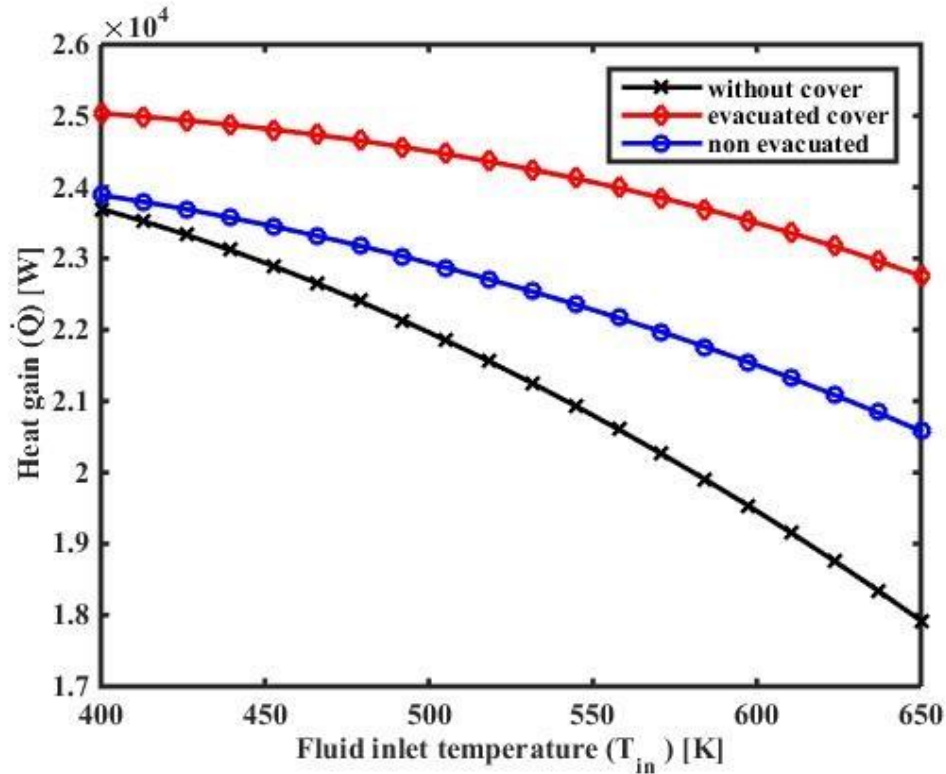


**Figure 5.20:** Heat gain as a function of fluid inlet temperature.

### 5.3.3 Effect of fluid inlet temperature on thermal efficiency

Thermal efficiency has been influencing the heat gain in every case and in all fluid inlet temperature range because of that thermal efficiency resulted as dividing the value of heat gain to the value of incoming solar irradiance onto the collectors. The magnitude of solar irradiance is constant but heat gain is decreasing with increasing fluid inlet temperature as shown in Figure 5.20'. Whereas the heat gains decrease for all cases as the thermal efficiency decline with it and get the same curve shape. Figure 5.21' explains thermal efficiency for evacuated cover in red, without cover in black and non-evacuated in blue.

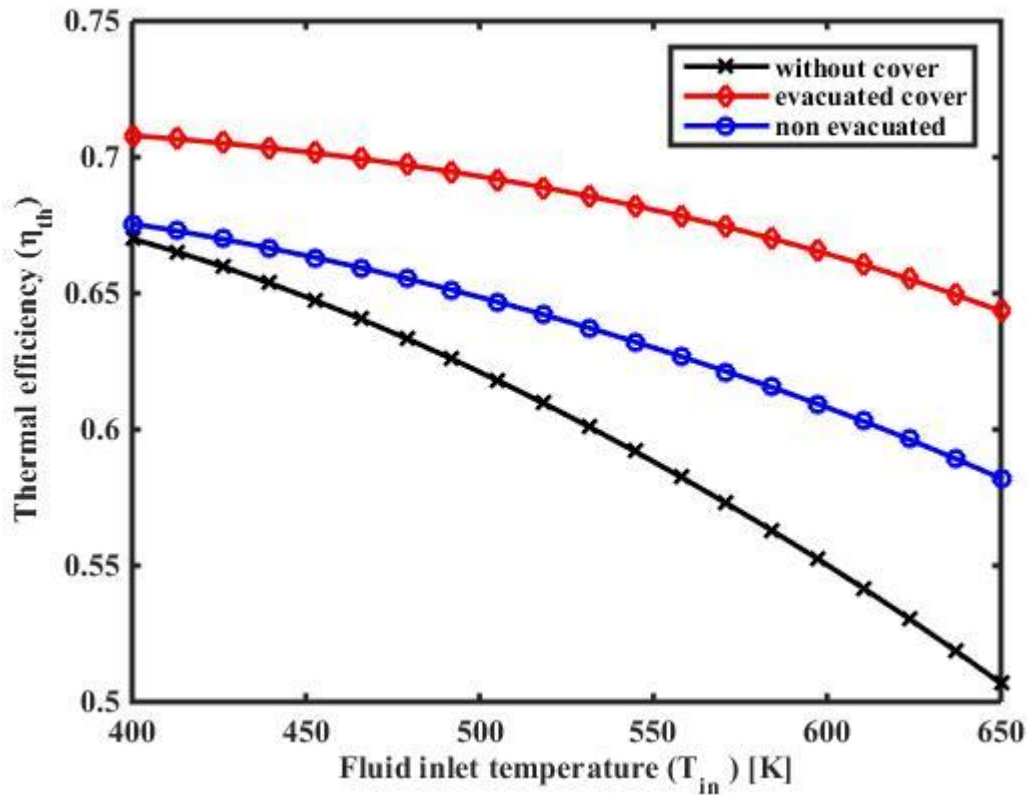


**Figure 5.21:** Thermal efficiency as a function of fluid inlet temperature.

## 5.4 Different solar radiation

### 5.4.1 Effect of solar radiation on outlet temperature

The same condition of verification have been considered for this case the only thing changed is that a wide range solar radiation between the minimum and maximum possible value ( $200-1200W/m^2$ ) has implemented in the calculation. The red curve from Figure 5.22' explains the highest value of outlet temperature for evacuated covered at all temperature range. Non-covered case by black curve shows the opposite of that happened in the evacuated. The blue curve denotes the non-evacuated case value which is near to the red curve at low solar radiation but it is approaching the black curve at high temperature it means that outlet temperature changing is varying for all cases.

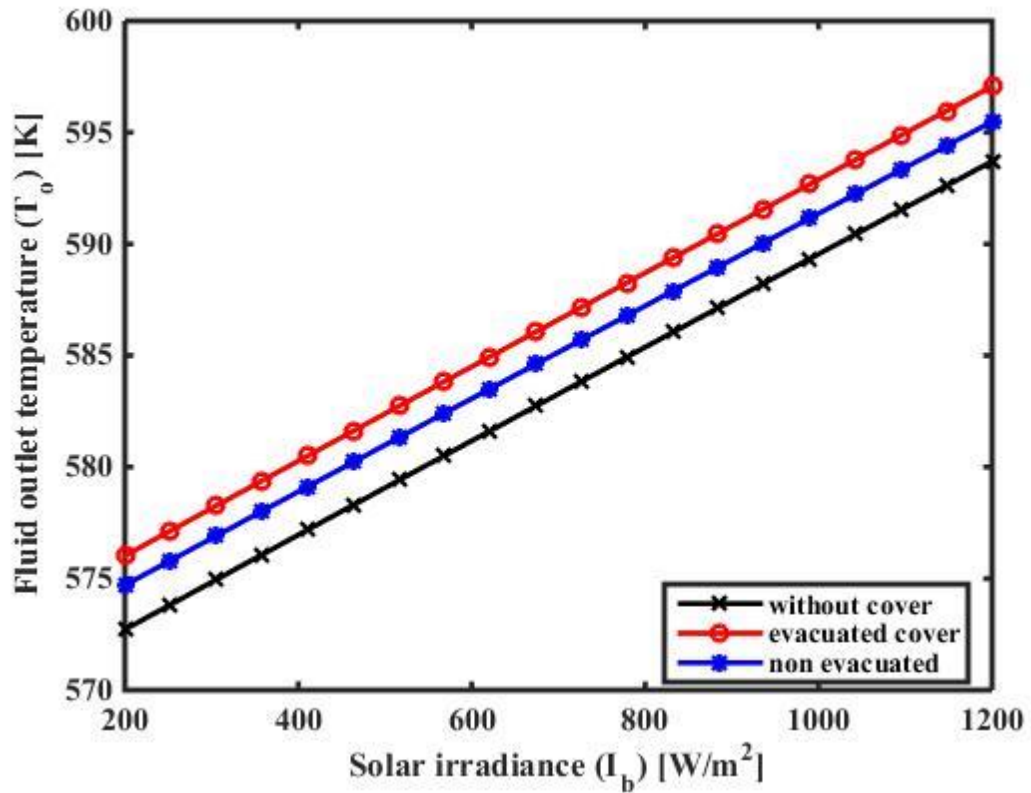
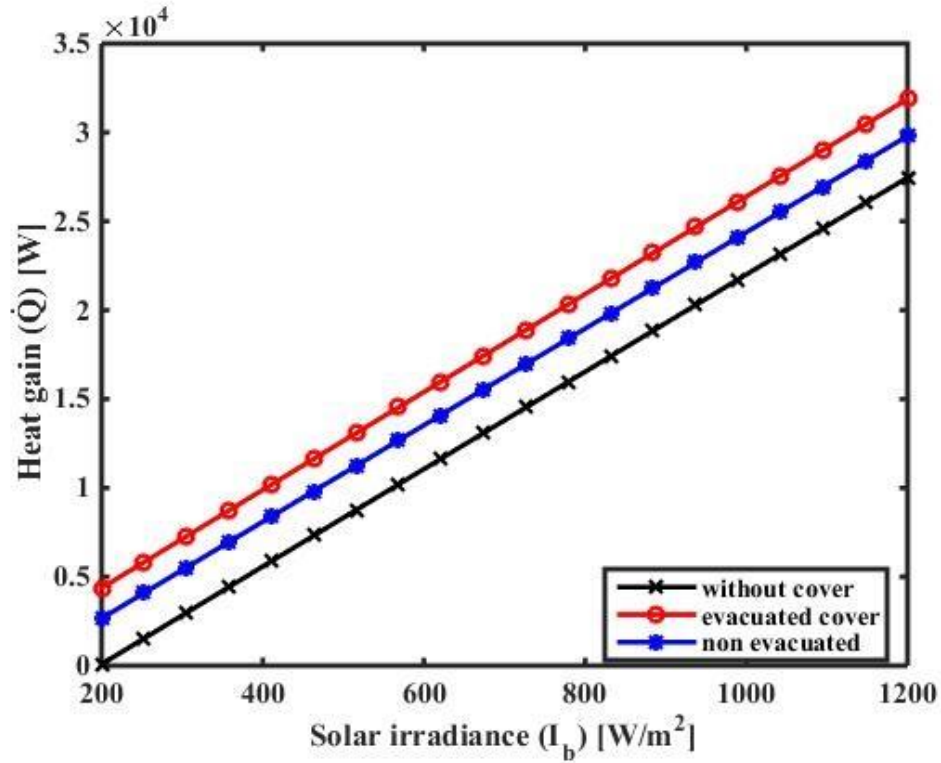


Figure 5.22: Fluid out let temperature as a function of solar radiation.

#### 5.4.2 Effect of solar radiation on the heat gain

In Figure 5.23' red, blue and black curves describing heat gained by the fluid with increasing solar irradiance for evacuated, non-evacuated and without cover cases, respectively. Heat gain is a product of specific heat by temperature different of Heat transfer fluid between outlet and inlet section. The changing in specific heat is very small in a compare with temperature difference so it has influenced temperature change with radiation that shown previously in Figure 5.22'.



**Figure 5.23:** Heat gain as a function of solar radiation.

### 5.4.3 Effect of solar radiation on thermal efficiency

Increasing solar irradiance have resulted increasing thermal efficiency. Figure 5.24' shows plotted curves for evacuated annular, the air in annular and coverless in red, blue and black colors, respectively for various range of solar radiation. Black curve refers to without cover case and has minimum value among them. Blue curve states air in the annular space case which is better than cover less collector. Red curve which is evacuated covered case has the maximum value than other cases and the most stable thermal efficiency with changing solar irradiance.

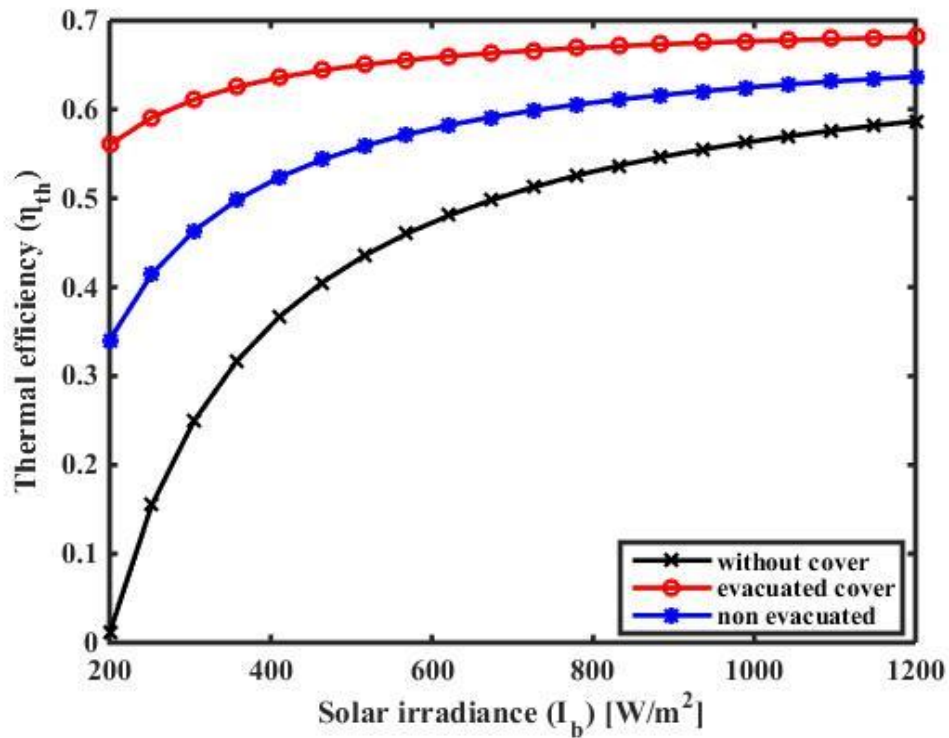


**Figure 5.24:** Effect of solar radiation in thermal efficiency.

## 5.5 Various volume flow rate

In this section all parameters have been assumed constant and same value of verification condition applied only change in the volume flow rate implemented in order to detect the investigation of improvement in thermal efficiency which is our goal. The volume flow rate in the verification was (55.4 l/min). The used range in this section is (10-90 l/min).

### 5.5.1 Impact of volume flow rate on outlet fluid temperature

Figure 5.25' shows the outlet temperature influencing volume flow rate for evacuated, non-evacuated and coverless. Respectively, in red, blue and black colors. The outlet temperature of fluid declining when its flow rates value growing. Whereas this decreasing have similarly shaped curves for all cases. The coverless case obtaining the highest outlet temperature and non-evacuated cover less than that. Finally, coverless has got less outlet temperature.

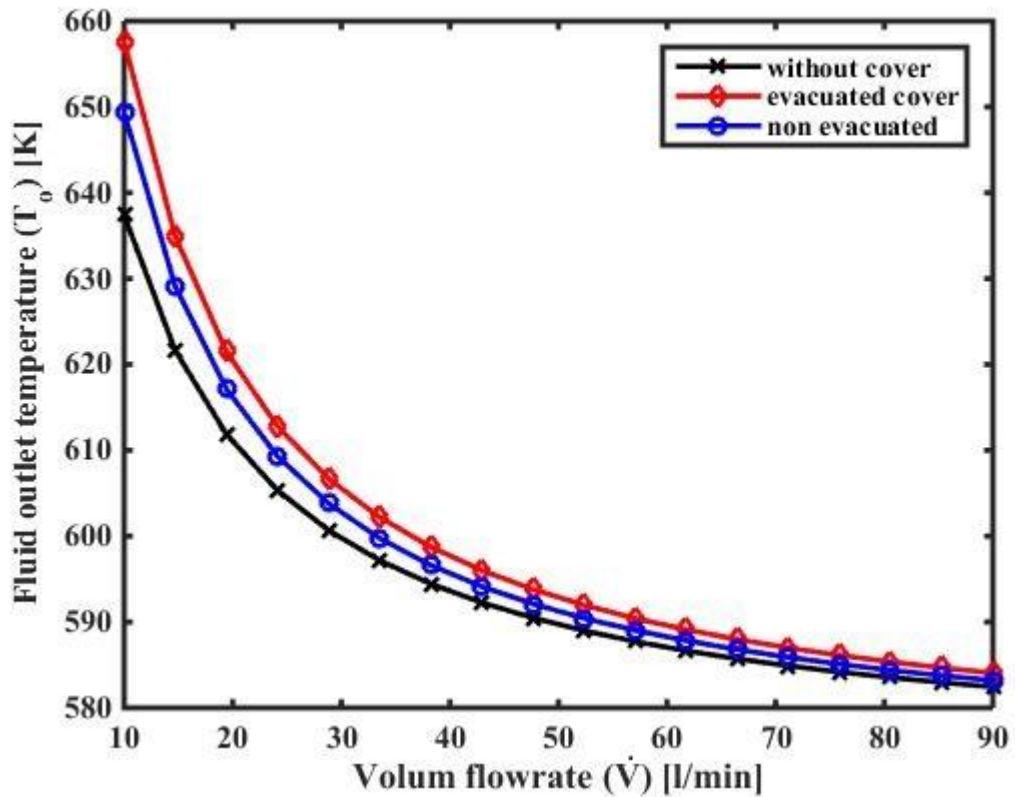


Figure 5.25: Fluid outlet temperature influencing various volume flow rate.

### 5.5.2 Impact of volume flow rate on heat gain

Enhancing heat transfer can be done by increasing volume flow rate of fluid this rising of the flow rate value leads to maximize Reynold number. Nusselt number changes directly proportional with Reynold number (Figure 5.14'), consequently they lead to get better heat transfer from the receiver tube wall to HTF. As explaining in the Figure 5.26' progressing in the value of volume flow rate resulting better heat transfer for present cases black, blue and red curves are demonstrating coverless, the air in the receiver cover space gap and no air in the gap between receiver and glass cover, respectively. It also improved that evacuated covered has the best heat gain between another.



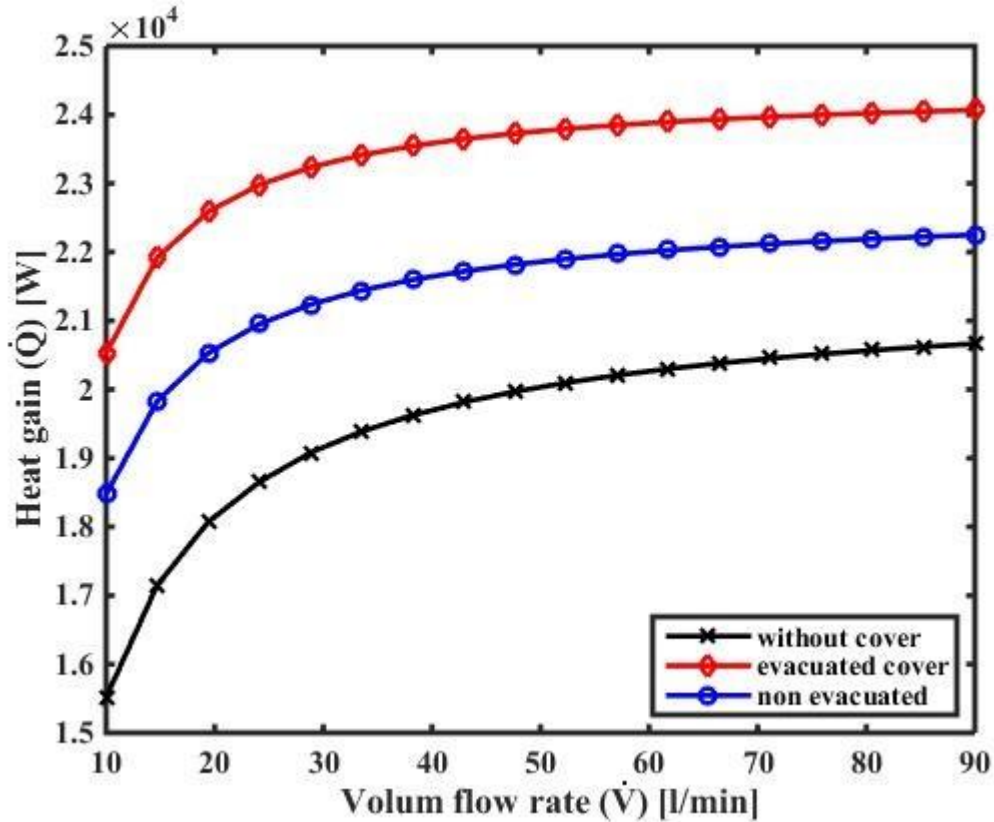
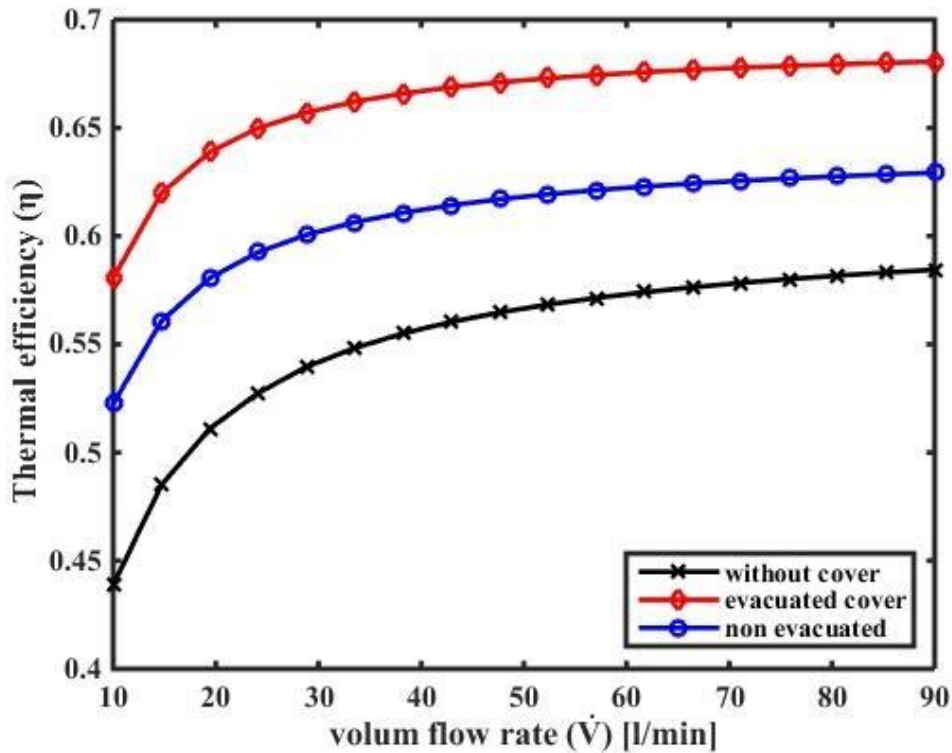


Figure 5.26: Heat gain influencing various volume flow rate.

### 5.5.3 Impact of volume flow rate on thermal efficiency and choosing an optimum case

Figure 5.27' showing the enhancement of thermal efficiency with cumulating the value of volume flow rate. Three simulated cases are showing in by red, blue and black colors. Thermal efficiency for evacuated one which is denoted by red curve has the highest influencing of volume flow rate at all range. After all these simulations steps the optimum case has been approved which evacuated tubular case has chosen as an optimum case among three simulated cases. This case has taken according to Figure 5.24' and Figure 5.27'.



**Figure 5.27:** Thermal efficiency with various volume flow rate for optimum case.

## 5.6 Addition of aluminum particles to the base fluid with various volume flow rate

As it shown before how the addition of nanoparticles improving the properties of fluid. So in the current study three different ratio added to the base fluid in order to obtain higher thermal efficiency and comparing to each other. The base fluid without powder is denoted by (0%) and three different ratio is (1%, 4% and 8%). On the other hand different volume flow rate between (44.5 (l/min) to 90 (l/min)) have used.

### 5.6.1 Effect of nanoparticles on fluid outlet temperature

The temperature of fluid outlet has been decreasing with increasing powders ratio in the base fluid for all range of inlet temperature. And it is decreasing with increasing volume flow rate as shown in Figure 5.28 (a)' for the inlet temperature (400 K), green line denoting Nano-fluid with 0.08 powder concentration when the outlet temperature is (421

K) at volume flow rate (44.5 (l/min)). It decreases to (410 K) at (90 (l/min)). It is a must of simulation to detect fluid outlet temperature since the operation temperature has limited and it should not exceed (673.15 K) which limited from manufactured data sheet. On the other hand by volume flow rate outlet temperature could be controlled that is why minimum possible volume flow rate which is (44.5 (l/min)) have been started with at (650K) inlet temperature according to Figure 5.28 (d)'. According to the fourth case ( $T_{in} = 650\text{K}$ ) range volume flow rate have taken for other cases.

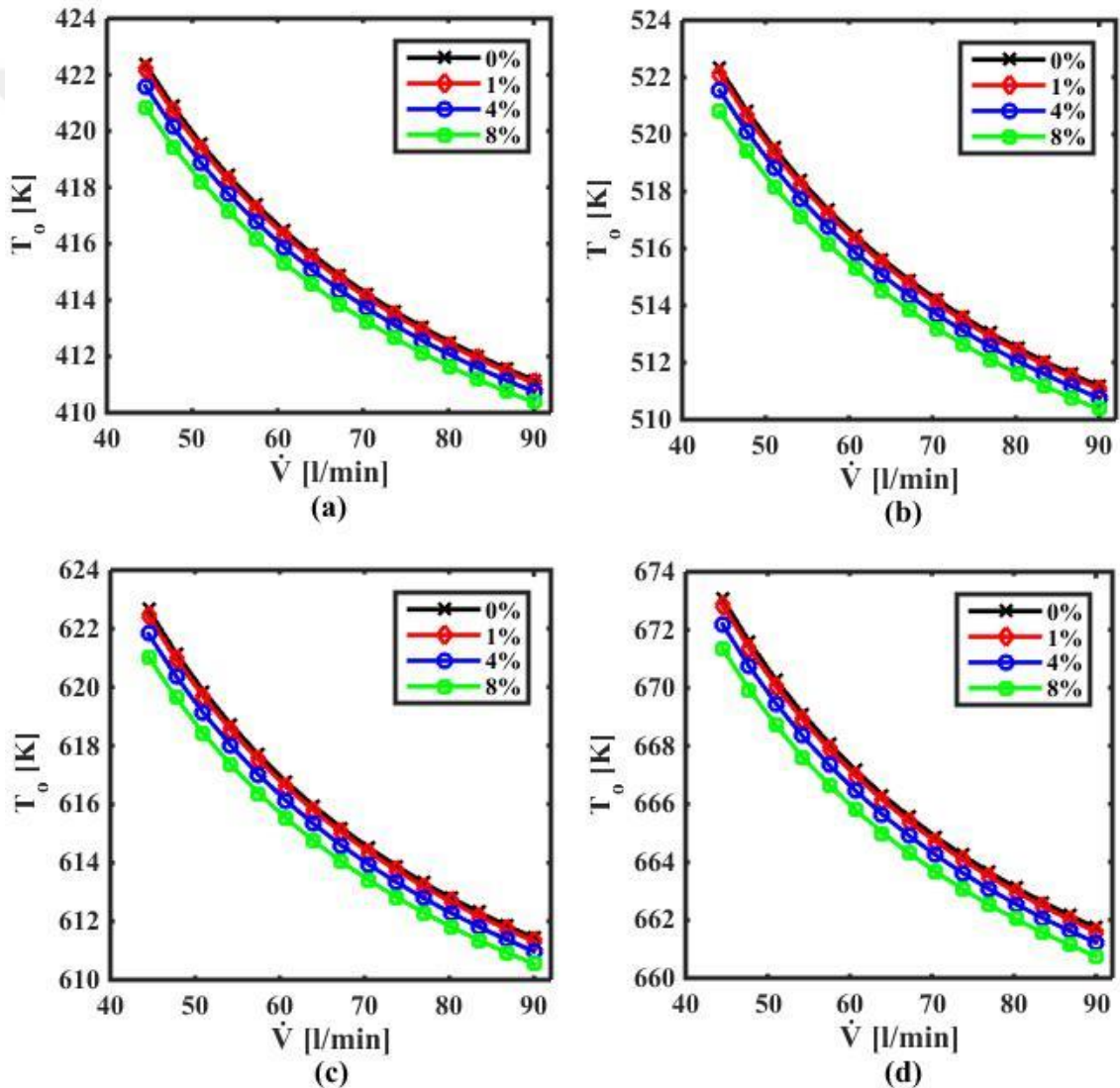


**Figure 5.28:** Fluid outlet temperature as a function of volume flow rate and powder concentration at inlet temperature of (a) 400 K, (b) 500 K, (c) 600 K and (d) 650 K.

### 5.6.2 Effect of nanoparticles on heat gain with various volume flow rate

Heat gain has estimated at the same range of volume flow rate for four different inlet temperature (400K, 500K, 600K and 650K). As clarifying in Figure 5.29' heat gain is increasing with flow rate cumulative. Also heat gain is declining with increasing fluid inlet temperature. For comparison in Figure 5.29 (b)' with Figure 5.29 (c)' the maximum value of heat gain at (90 (l/min)) for (0.08) powder concentration have declined from ( $2.47 \times 10^4$ ) at ( $T_{in} = 500K$ ) to ( $2.36 \times 10^4$ ) at ( $T_{in} = 600K$ ). Even though heat gain is decreasing with increasing inlet temperature the effect of nanoparticles become greater. For example, in Figure 5.29 (b)' the different between the different curves for (0%, 1%, 4% and 8%) does not appeared clearly but this different is very clear at Figure 5.29 (d)' that is because of impact of aluminum partials which means that nanoparticles enhanced heat transfer. The effect of different ratio of aluminum powder can be seen well in the Figure 5.30' which is enlarged section for Y-axis only.

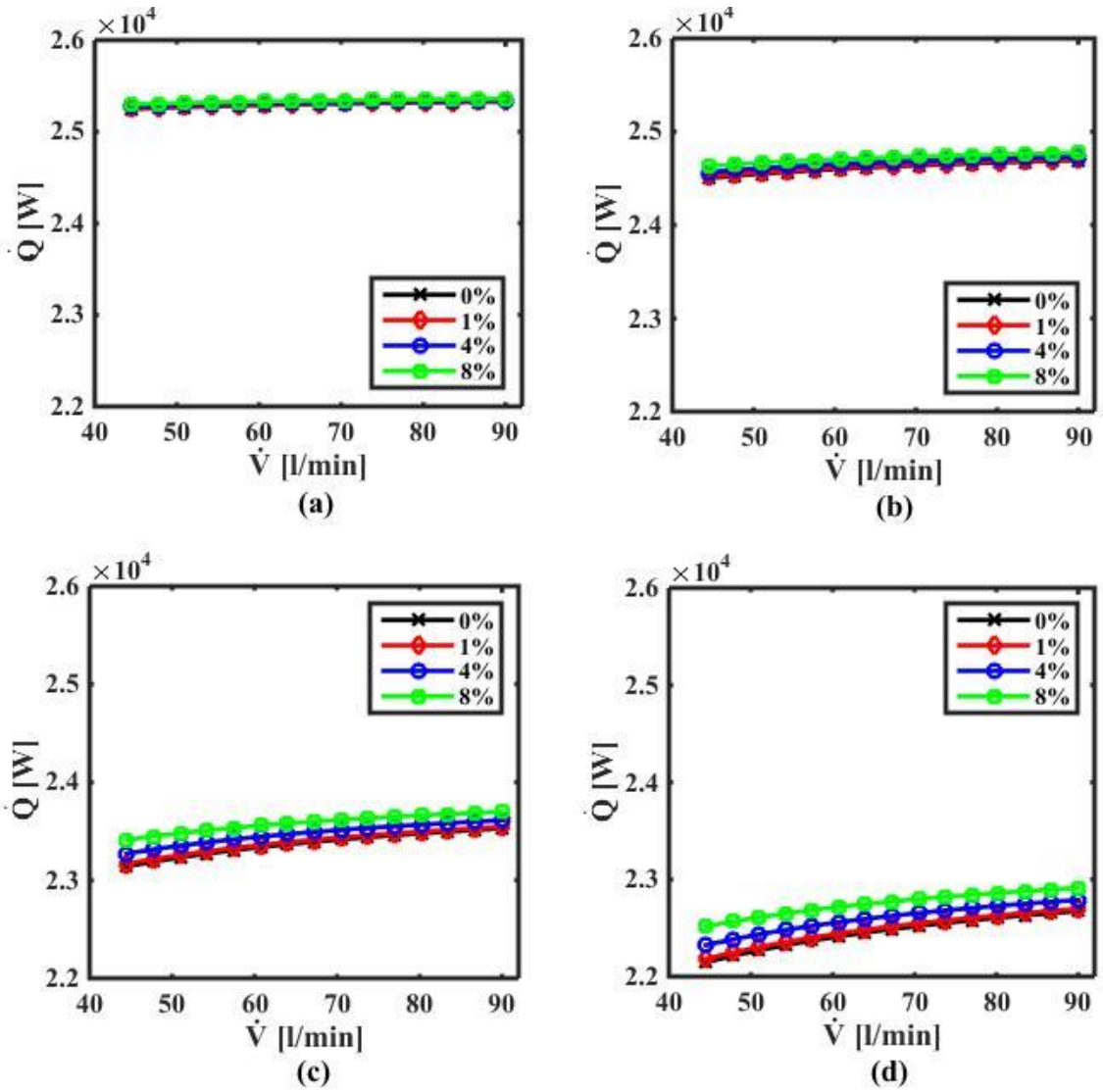


**Figure 5.29:** Useful heat gain as a function of volume flow rate and powder concentration at inlet temperature of (a) 400 K, (b) 500 K, (c) 600 K and (d) 650 K.

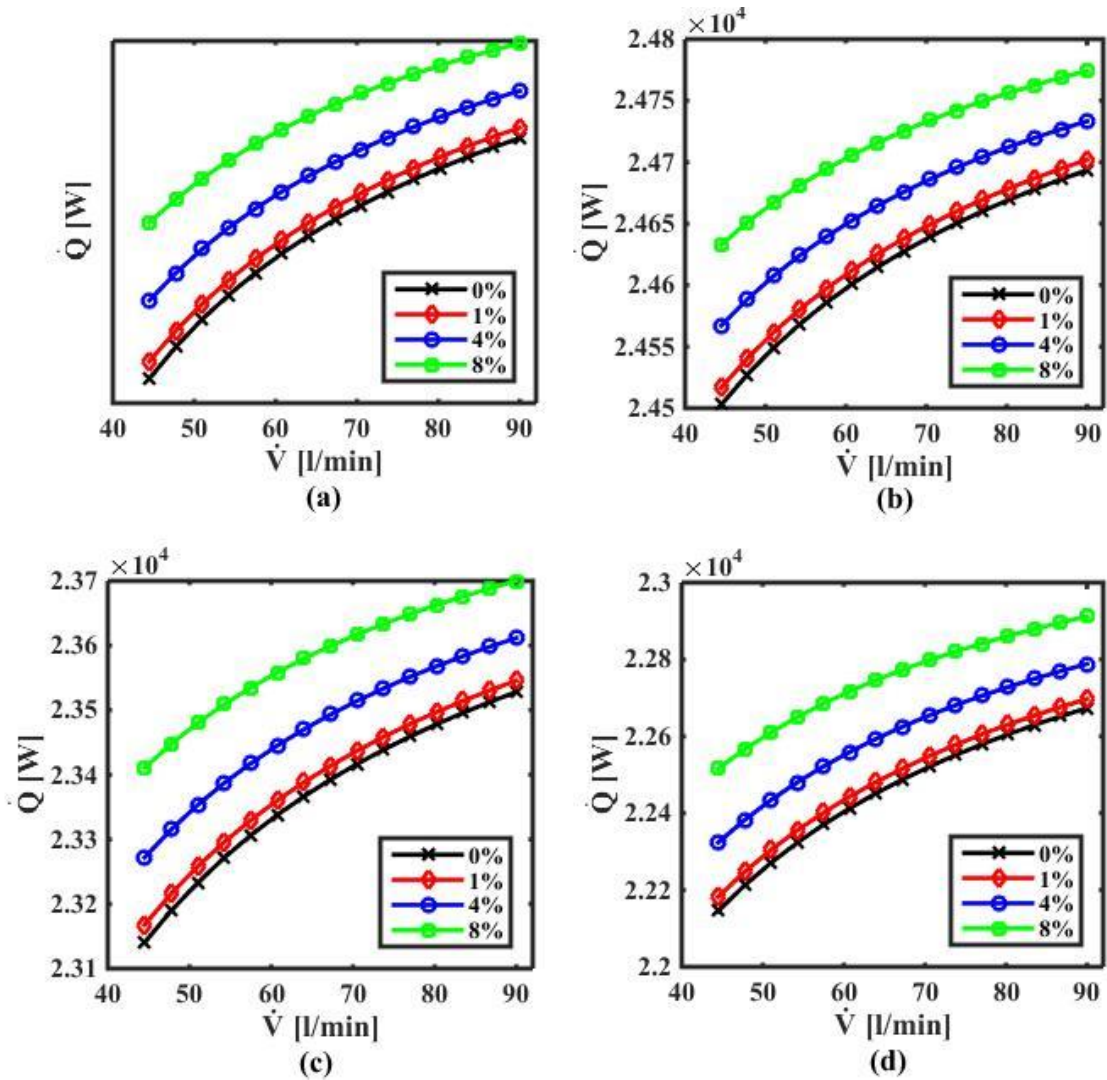
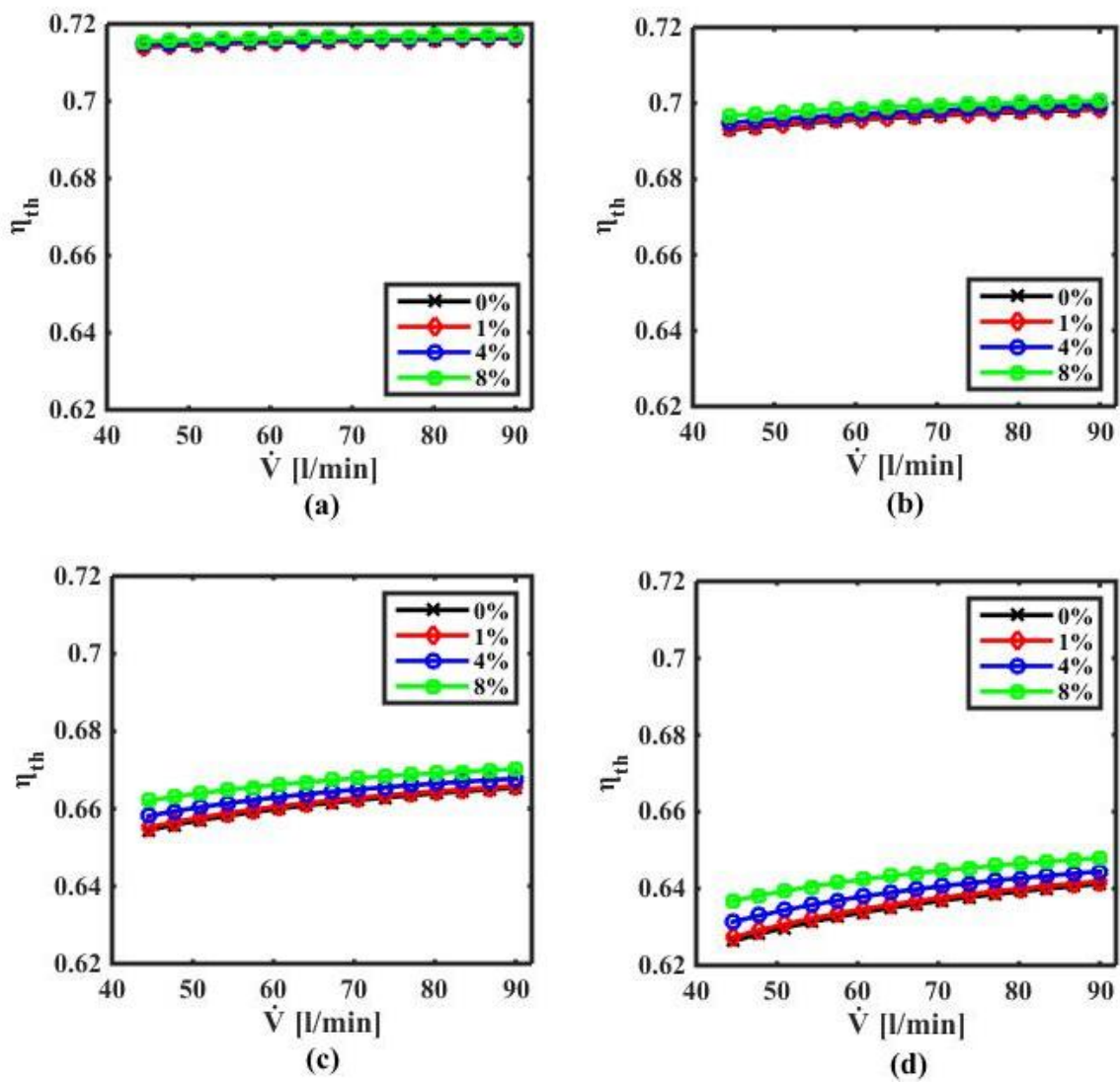


Figure 5.30: enlarged sections of Figure 5.29' for Y-axis only.

### 5.6.3 Effect of nanoparticles on thermal efficiency with range of volume flow rate

In spite of growing in the value of thermal efficiency by increasing volume flow rate. Powders concentration has a great effect on thermos-physical properties of fluid which leads to obtain better heat transfer, consequently, enhancement in thermal efficiency occur. Thermal efficiency enhancement by aluminum powder has become higher with rising fluid outlet temperature. On the other hand, fluid inlet temperature effect negatively on the thermal efficiency. In Figure 5.31', the maximum value of thermal efficiency are (71.5, 70.7, 67.04 and 64.9) at ( $\dot{V} = 90(l / \text{min})$ ) for (0.08) powder concentration for fluid inlet temperature (400K, 500K, 600K and 650K), respectively which decreased with

increasing inlet temperature. But the improving of thermal efficiency by nanoparticles concentration at the same temperature of fluid have been taking place as clarified in Figure 5.31(a)' to Figure 5.31(d)'. For instant Figure 5.31 (a)' when the operation temperature is (400K) the effect of powder is very small and the curves are very close to each other. The space between the curves growing with raising the operating temperature as it shown in Figure 5.31(d)' in which the increasing of thermal efficiency happened by adding more powder to the base fluid at ( $\dot{V} = 90(l/min)$ ) from (0.641) for base fluid to (0.648) for powder ratio (0.08). And the results shown better in the Figure 5.32'.



**Figure 5.31:** Thermal efficiency as a function of volume flow rate and powder concentration at inlet temperature of (a) 400 K, (b) 500 K, (c) 600 K and (d) 650 K.

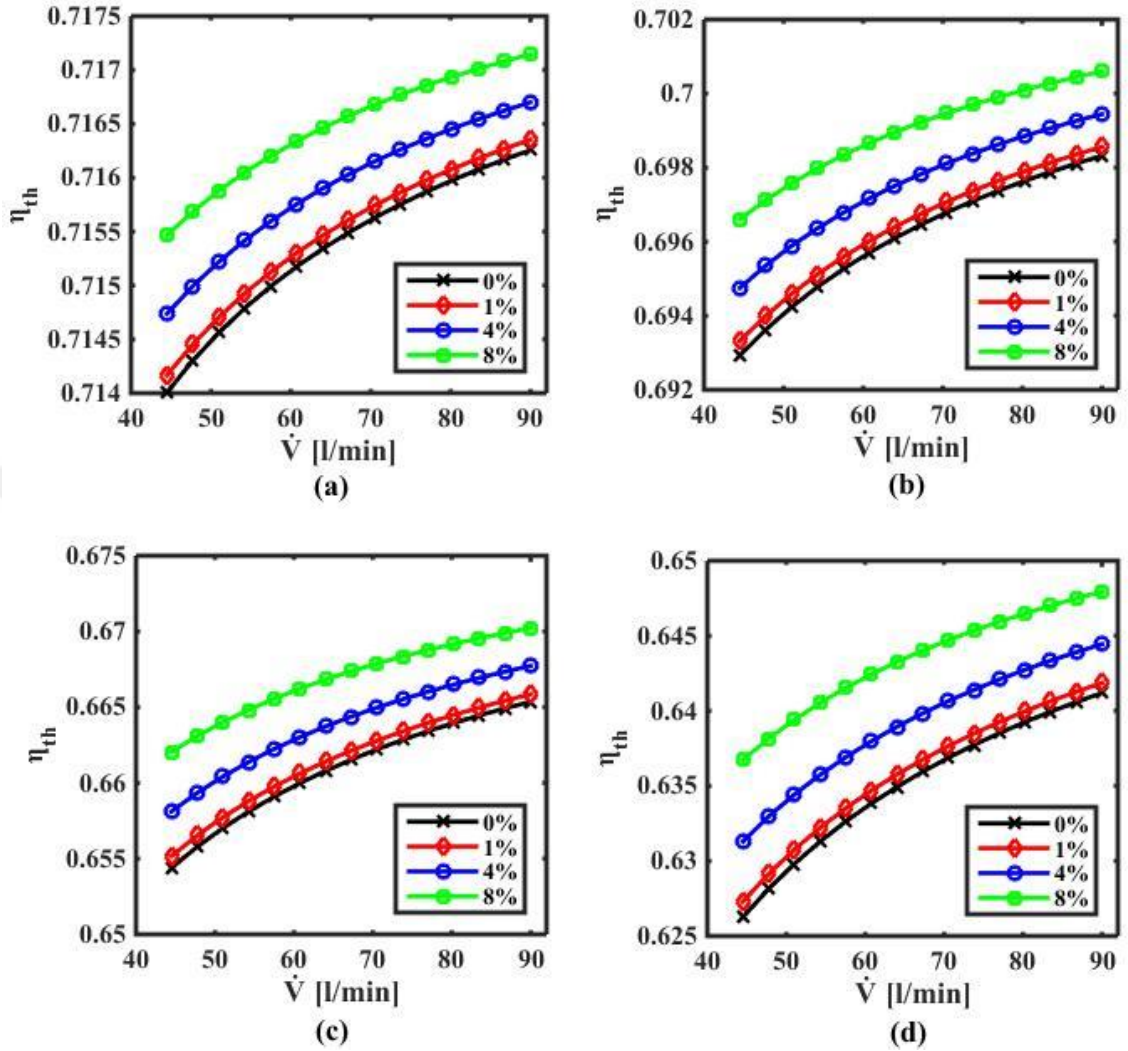


Figure 5.32: enlarged sections of Figure 5.31' for Y-axis only.

## 5.7 Various range of Reynold number

### 5.7.1 Effect of Reynold number fluid outlet temperature with different powder concentration

Figure 5.33' shows the influencing of outlet temperature by Reynold number for four assumed inlets fluid temperature as shown in Figure 5.33' (a, b, c and d), respectively. In each part of the figure (black, red, blue and green) colors curves expressing (0%, 1%, 4% and 8%) powder ratio one-to-one. For all cases outlet temperature of fluid declining when



its Reynold numbers value growing. Whereas highest powder ratio obtaining the lowest fluid outlet temperature. Outlet fluid temperature is the most important parameter for the current study and it must not exceed the limited range (673.15 K). In Figure 5.33' (d)' for not exceeding limited range of base fluid temperature, the higher Reynold number have assumed where the inlet temperature is (650 K). The effect of powder addition is appeared by decreasing the outlet temperature into limited range and it is a good advantage in operation with high temperature.

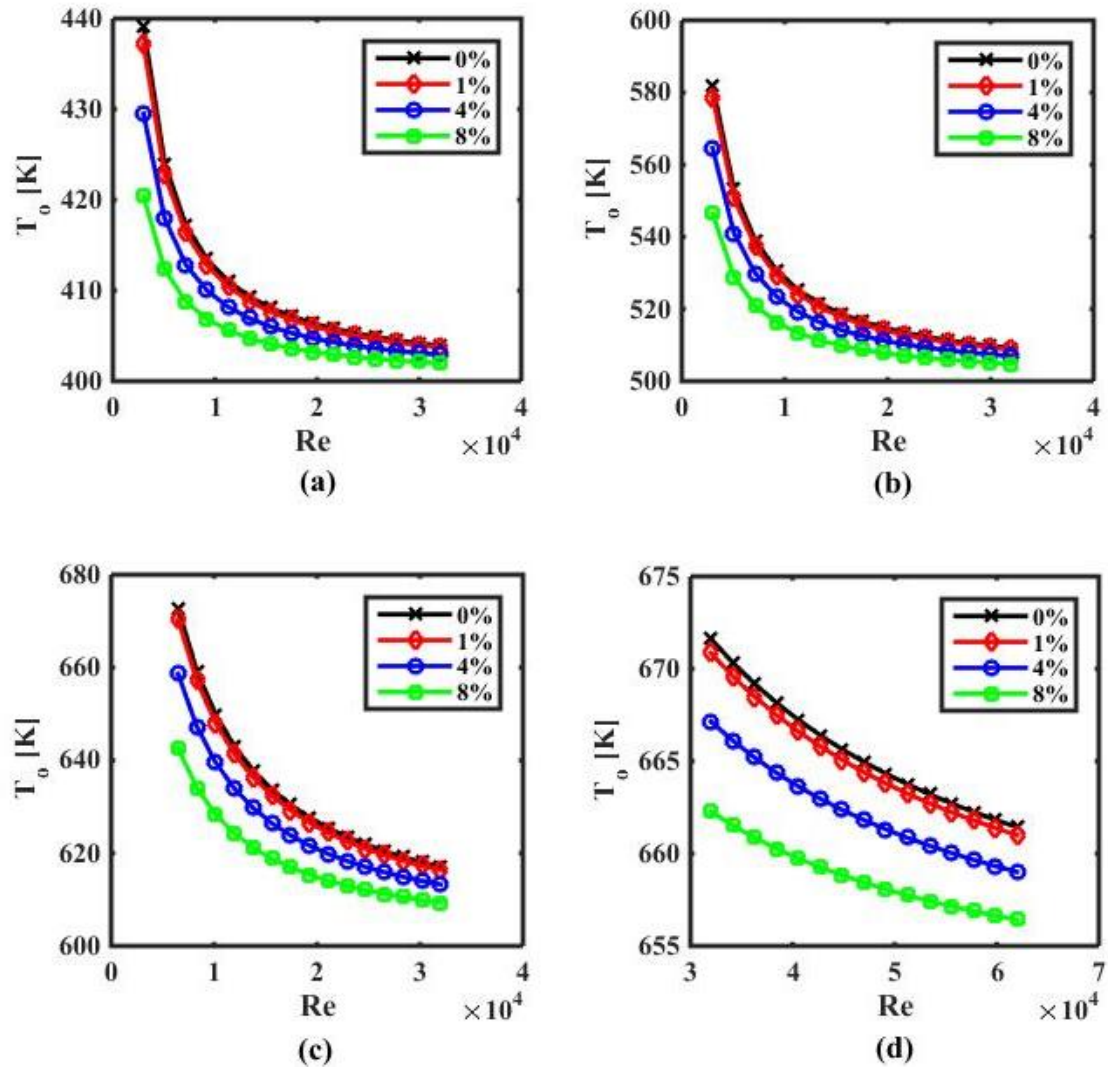


**Figure 5.33:** Fluid outlet temperature as a function of Reynold number and powder concentration at inlet temperature of (a) 400 K, (b) 500 K, (c) 600 K and (d) 650 K.

### **5.7.2 Effect of aluminum powder on the useful heat gain with range of Reynold number**

Figure 5.34' is explaining the influencing of heat gain for four different cases (a, b, c, and d) for the fluid inlet temperature of (400 K, 500 K, 600 K and 650K) respectively. In all cases of fluid inlet temperature, the highest ratio of powder concentration the heat gain has the greatest value. Despite rising the value useful energy gain by fluid by adding more aluminum powder but the effect of powder concentration decreasing by increasing Reynold number for instant, in Figure 5.34 (c)' the deferent between green and blue curves in low Reynold number is greater than in the higher Reynold number. On the other hand, increasing fluid inlet temperature leads to decrease the amount of heat gain. For example, in Figure 5.34 (a)' and Figure 5.34 (b) the maximum heat gain by the Nano-fluid with a concentration ratio (8%) which is denoted by green line at Reynold number (32000) are  $(2.397 \times 10^4)$  and  $(2.485 \times 10^4)$  respectively.

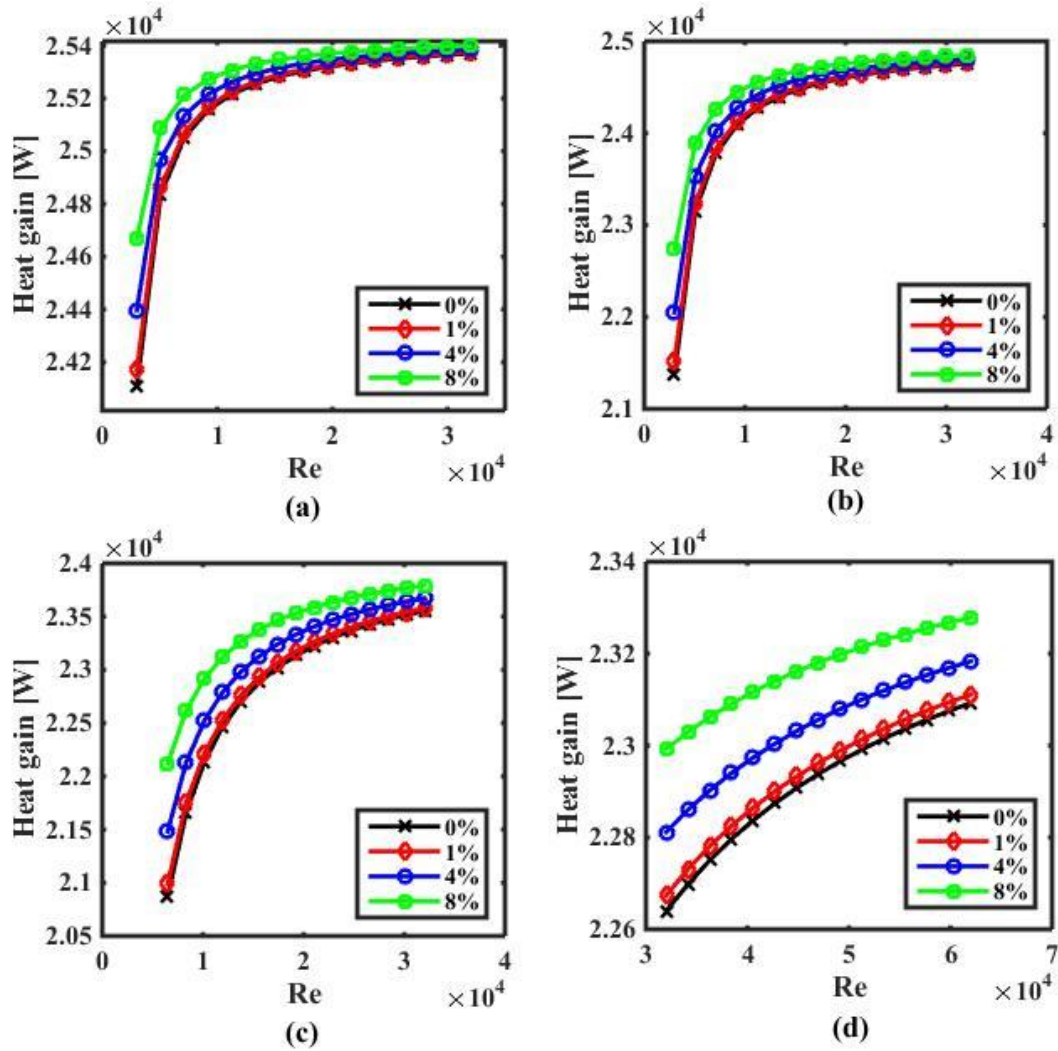


**Figure 5.34:** Useful heat gain as a function of Reynolds number and powder concentration at inlet temperature of (a) 400 K, (b) 500 K, (c) 600 K and (d) 650 K.

### 5.7.3 Enhancement investigation of thermal efficiency by powder concentration with a range of Reynold number.

Considering Reynold number at the inlet section have assumed for investigation of improvement thermal efficiency by adding aluminum oxide nanoparticles. A wide range of Reynold number at the inlet of receiver tube has been assumed. As shown in Figure 5.35' four cases have assumed from (a to d) for (400K, 500K, 600K, and 650K) respectively. Green curve defines thermal efficiency with the maximum value of powder ratio (8%) in the base fluid which has the highest thermal efficiency. The black curve

which contains on powder has had the lowest thermal efficiency. The thermal efficiency of (4%) powder ratio is appearing by the blue curve which its thermal efficiency is less than (8%) powder concentration and red curve denoting (1%) powder concentration which is between black and blue curves that clearly shown in Figure 5.35(d)'. The effect of nanoparticles on rising thermal efficiency at lower Reynold number and lower fluid inlet temperature is greater. Even though nanoparticles addition effect positively on thermal efficiency, The impact of aluminum powders ratio become less and less as the value of Reynold number became more and more.

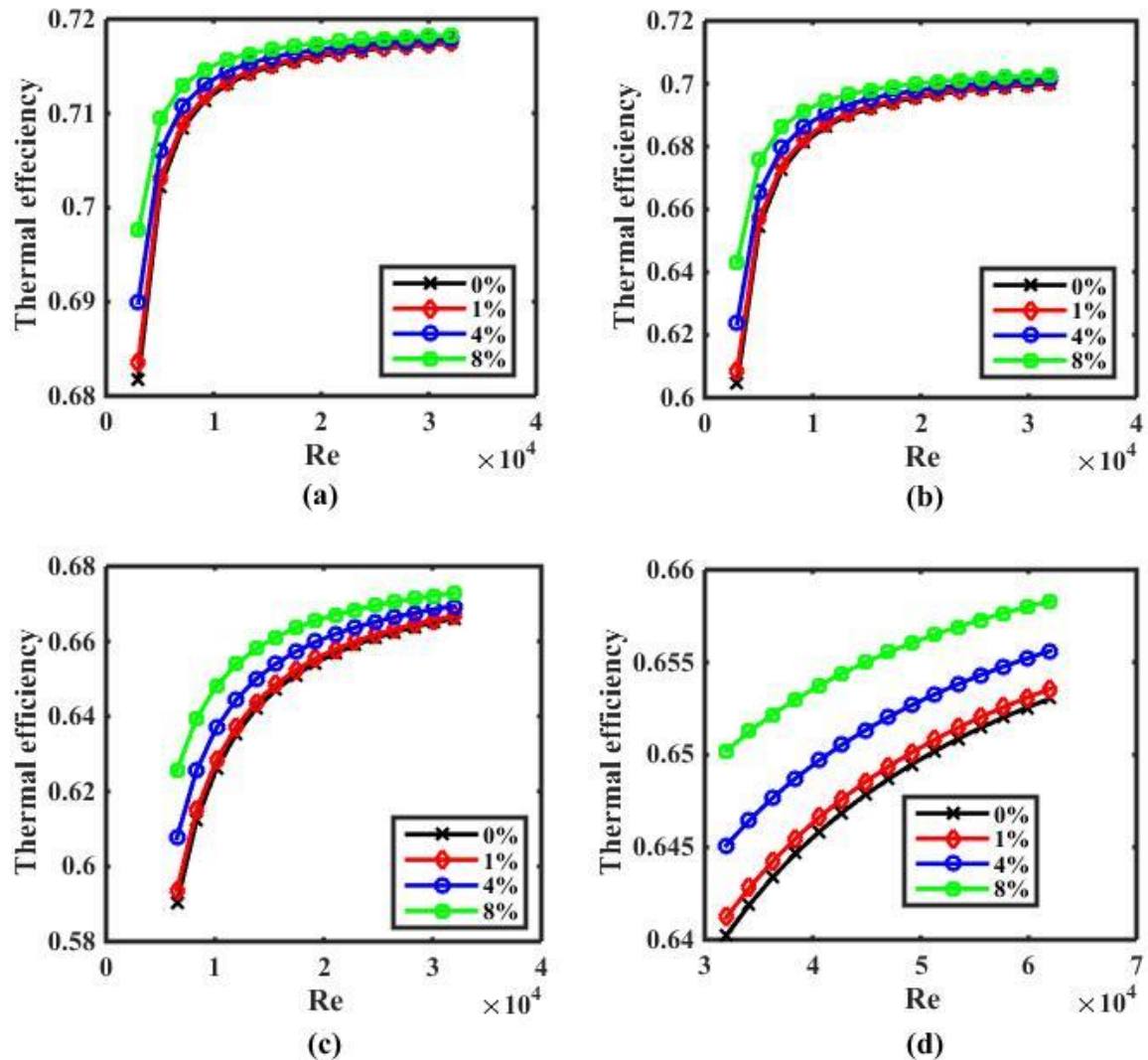


**Figure 5.35:** Thermal efficiency as a function of Reynolds number and powder concentration at inlet temperature of (a) 400 K, (b) 500 K, (c) 600 K and (d) 650 K.

# CHAPTER SIX

## CONCLUSION AND FUTURE WORK

### 6.1 Conclusion

The purpose of the study is to improve the thermal performance of parabolic trough collector at the maximum possible temperature of inlet fluid at steady state condition for three cases (without cover, non-evacuated and evacuate covered). At the beginning, the properties of Nano-fluid as a function of volumetric powder concentrating in the base fluid and as a function of temperature have defined in the code. Then the discretized equation of finite volume method was simulated by using MATLAB software.

First: a numerically simulated result have taken for non-evacuated case. Along the collector fluid, receiver and glass cover temperature found in addition of useful heat gain and heat loss. After that thermal efficiency have found and compared with experimental result the difference in was (0.9%).

Second: it is proved that increasing solar radiation and volume flow rate enhancing heat transfer and improving thermal efficiency for three cases. For evacuated case, as solar radiation ( $200 \text{ W/m}^2$ ) thermal efficiency is (56.03%) and becomes (68.12%) when radiation is ( $1200 \text{ W/m}^2$ ). When volume flow rate increased (from 10 l/min to 90 l/min) thermal efficiency enhanced (from 58.05% to 68.06%). But increasing fluid inlet temperature has negative effect on thermal efficiency. The optimum case which is evacuated covered was selected according to obtained results.

Third: addition of nanoparticles had increased thermal efficiency at all volume flow rate and all temperature range but the effect of powder have been increasing with rising operating temperature. As operating temperature is (650K) and volume flow rate (90 l/min) thermal efficiency was (0.641 %) for (0 %) powder concentration and its value increased to (0.648 %) for (8%) powder concentration. But at the low operation

temperature the effect of powder concentration was smaller than high operating temperature.

Fourth: when Reynold number assumed at inlet section. Its minimum value changing according to the outlet temperature for staying at temperature lower than (673.15K) which is our limit range. Especially at high operating temperature higher Reynold number should be used.

### **Future Work**

As extension for this study, other types of powder with different size can be used instead of aluminum nanoparticles

It can be the basic component for solar power plant design with using analyzed data of solar radiation for certain place such as Iraq.

## Appendix (A)

### Air properties

Air properties as a function of temperature are changing. The correlations which depend by different polynomials for each property can be applied to a wide range of temperature. From 150 K to 3000 K these equations can be used [37].

#### Density

$$\rho = 345.57(T - 2.6884)^{-1} \quad (1)$$

#### Dynamic viscosity

$$\mu = 2.5914 \times 10^{-15} \times T^3 - 1.4346 \times 10^{-11} \times T^2 + 5.0523 \times 10^{-8} \times T + 4.113 \times 10^{-6} \quad (2)$$

#### Thermal conductivity

$$k = 1.5797 \times 10^{-17} \times T^5 - 9.4600 \times 10^{-14} \times T^4 + 2.2012 \times 10^{-10} \times T^3 - 2.3758 \times 10^{-7} \times T^2 + 1.7082 \times 10^{-4} \times T - 7.488 \times 10^{-3} \quad (3)$$

#### Prandtl number

$$\text{Pr} = 1.0677 \times 10^{-23} \times T^7 - 7.6511 \times 10^{-20} \times T^6 + 1.0395 \times 10^{-16} \times T^5 + 4.6851 \times 10^{-13} \times T^4 - 1.7698 \times 10^{-9} \times T^3 + 2.2260 \times 10^{-6} \times T^2 - 1.1262 \times 10^{-3} \times T + 0.88353 \quad (4)$$

## References

1. Alfellag, M.A.A., <Modeling and Experimental Investigation of Parabolic Trough Solar.pdf>, in Department of Mechanical Engineering. 2014, Embry-Riddle Aeronautical University, Daytona Beach, Florida.
2. Muñoz, J. and A. Abánades, Analysis of internal helically finned tubes for parabolic trough design by CFD tools. *Applied Energy*, 2011. 88(11): p. 4139-4149.
3. He, Y.-L., et al., A MCRT and FVM coupled simulation method for energy conversion process in parabolic trough solar collector. *Renewable Energy*, 2011. 36(3): p. 976-985.
4. Kalogirou, S.A., Solar thermal collectors and applications. *Progress in Energy and Combustion Science*, 2004. 30(3): p. 231-295.
5. Liu, X., J. Huang, and Q. Mao, Sensitive Analysis for the Efficiency of a Parabolic Trough Solar Collector Based on Orthogonal Experiment. *International Journal of Photoenergy*, 2015. 2015: p. 7.
6. Bellos, E., C. Tzivanidis, and K.A. Antonopoulos, A detailed working fluid investigation for solar parabolic trough collectors. *Applied Thermal Engineering*, 2017. 114: p. 374-386.
7. Sharma, K., et al., A Review on the Performance of the Nanofluid Based Solar Collectors-Solar Energy. *ELK Asia Pacific Journals–Special Issue*, 2015. 1(1): p. 201-212.
8. Mwesigye, A., et al., THERMAL EFFICIENCY AND ENTROPY GENERATION FOR A PARABOLIC TROUGH RECEIVER AT DIFFERENT CONCENTRATION RATIOS.
9. Mwesigye, A., Z. Huan, and J.P. Meyer, Thermodynamic optimisation of the performance of a parabolic trough receiver using synthetic oil–Al<sub>2</sub>O<sub>3</sub> nanofluid. *Applied Energy*, 2015. 156: p. 398-412.
10. García-Valladares, O. and N. Velázquez, Numerical simulation of parabolic trough solar collector: Improvement using counter flow concentric circular heat exchangers. *International Journal of Heat and Mass Transfer*, 2009. 52(3–4): p. 597-609.



11. Hadj Ammar, M.A., B. Benhaoua, and M. Balghouthi, Simulation of tubular adsorber for adsorption refrigeration system powered by solar energy in sub-Saharan region of Algeria. *Energy Conversion and Management*, 2015. 106: p. 31-40.
12. Zheng, Z., Y. Xu, and Y. He, Thermal analysis of a solar parabolic trough receiver tube with porous insert optimized by coupling genetic algorithm and CFD. *Science China Technological Sciences*, 2016. 59(10): p. 1475-1485.
13. Ghasemi, S.E., A.A. Ranjbar, and A. Ramiar, Three-dimensional numerical analysis of heat transfer characteristics of solar parabolic collector with two segmental rings. *J Math Comput Sci*, 2013. 7: p. 89-100.
14. Tzivanidis, C., et al., Thermal and optical efficiency investigation of a parabolic trough collector. *Case Studies in Thermal Engineering*, 2015. 6: p. 226-237.
15. KUMAR SUNIL, L.K., SHARMA SUMEET, PERFORMANCE EVALUATION OF A NANOFLUID BASED PARABOLIC SOLAR COLLECTOR – AN EXPERIMENTAL STUDY. *International Journal of Mechanical And Production Engineering*, ISSN: 2320-2092,, 2014.
16. Charalambous, P.G., et al., Photovoltaic thermal (PV/T) collectors: A review. *Applied Thermal Engineering*, 2007. 27(2–3): p. 275-286.
17. Thirugnanasambandam, M., S. Iniyar, and R. Goic, A review of solar thermal technologies. *Renewable and Sustainable Energy Reviews*, 2010. 14(1): p. 312-322.
18. Tyagi, V.V., S.C. Kaushik, and S.K. Tyagi, Advancement in solar photovoltaic/thermal (PV/T) hybrid collector technology. *Renewable and Sustainable Energy Reviews*, 2012. 16(3): p. 1383-1398.
19. Silva, J.P., Modelling and Simulation of Parabolic Trough Power Plant.
20. HARPER, G.D.J., *Solar\_Energy\_Projects\_for\_the\_Evil\_Genius*. McGraw-Hill, 2007.
21. Hachicha, A.A., Numerical modelling of a parabolic trough solar collector. 2013.
22. null, W.K., H.Y. null, and C.Z. null, A design method and numerical study for a new type parabolic trough solar collector with uniform solar flux distribution. *SCIENCE CHINA Technological Sciences*, 2014. 57(3): p. 531.

23. Canavarro, D., J. Chaves, and M. Collares-Pereira, New Optical Designs for Large Parabolic Troughs. *Energy Procedia*, 2014. 49: p. 1279-1287.
24. Forristall, R., Heat Transfer Analysis and Modeling of a Parabolic Trough Solar Receiver Implemented in Engineering Equation Solver. 2003: National Renewable Energy Laboratory.
25. Guo, J., X. Huai, and Z. Liu, Performance investigation of parabolic trough solar receiver. *Applied Thermal Engineering*, 2016. 95: p. 357-364.
26. Dharmalingam, R., K. Sivagnanaprabhu, and S. Periyasamy, EXPERIMENTAL INVESTIGATION AND MATHEMATICAL STUDY OF PERFORMANCE CHARACTERISTICS OF SOLAR FLAT PLATE COLLECTOR USING  $Al_2O_3$ /WATER NANO FLUID.
27. Said, Z., et al., Performance enhancement of a Flat Plate Solar collector using Titanium dioxide nanofluid and Polyethylene Glycol dispersant. *Journal of Cleaner Production*, 2015. 92: p. 343-353.
28. Verma, S.K., A.K. Tiwari, and D.S. Chauhan, Experimental evaluation of flat plate solar collector using nanofluids. *Energy Conversion and Management*, 2017. 134: p. 103-115.
29. Ekramian, E., S.G. Etemad, and M. Haghshenasfard, Numerical Investigations of Heat Transfer Performance of Nanofluids in a Flat Plate Solar Collector. *Journal ISSN*, 2014. 1929: p. 1248.
30. Manca, O., et al., Numerical study of a confined slot impinging jet with nanofluids. *Nanoscale Res Lett*, 2011. 6(1): p. 188.
31. Li, P., D. Zhang, and Y. Xie, Heat transfer and flow analysis of  $Al_2O_3$ -water nanofluids in microchannel with dimple and protrusion. *International Journal of Heat and Mass Transfer*, 2014. 73: p. 456-467.
32. Ho, C.J., Numerical Simulation of Natural Convection of Nanofluid in a Square Enclosure: Effects Due To Uncertainties of Viscosity and Thermal Conductivity. *International Journal of Heat and Mass Transfer*, 2008.
33. Marif, Y., et al., Numerical simulation of solar parabolic trough collector performance in the Algeria Saharan region. *Energy Conversion and Management*, 2014. 85: p. 521-529.

34. YUNUS A. ÇENGEL, A.J.G., Heat and Mass Transfer Fundamentals and Applications 5th ed by Yunus A. Cengel. Vol. 5th. 2008: McGraw-Hill Education.
35. Jiji, L.M., Heat Convection. 2009.
36. Mwesigye, A., T. Bello-Ochende, and J.P. Meyer, Heat transfer and thermodynamic performance of a parabolic trough receiver with centrally placed perforated plate inserts. Applied Energy, 2014. 136: p. 989-1003.
37. Zografos, A.I., W.A. Martin, and J.E. Sunderland, Equations of properties as a function of temperature for seven fluids. Computer Methods in Applied Mechanics and Engineering, 1987. 61(2): p. 177-187.

## **CURRICULUM VITAE (C.V.)**

### **PERSONAL INFORMATION:**

**Full Names:** Rahell Nasruldeen Mohammed

**Gender:** Male

**Marital Status:** married

**Nationality:** Iraqi

**City and Date of Birth:** Kirkuk- 12.04.1989

**Address:** gazi mahallesi, senol caddesi, 100/2, yenimahalle Ankara

**Mobile Number:** 00905385900141

**E-mail address:** [rahell.sharmin@gmail.com](mailto:rahell.sharmin@gmail.com)



### **EDUCATION :**

**High School:** Kurdistan High School

**Bachelor:** Fuel & Energy Engineering Technique- Kirkuk Technology College

### **WORK EXPERIENCES:**

#### **First Job:**

Working at Kat refinery plant for asphalt and luboil (vacuum system) as operator engineer / Kirkuk / Iraq 2011-2013

#### **Second Job:**

Responsible of distillation unit (atmospheric system) and penal control room operator at Bazian refinery /Sulaimania /Iraq 2013-2014.

#### **Training Courses:**

Two months Training at Iraqi North's Oil Company/ Kirkuk.

Two months Training at Iraqi North's Gas Company/ Kirkuk.

#### **Undergraduate Graduation Project:**

Designing of House Depending on Solar Energy.